The effect of zinc as a nonmagnetic impurity on high-temperature superconducting cuprates

Silke Schönecker

Master Thesis

Supervised by
Prof. Cristiane de Morais Smith
Prof. Lizardo Nunes

July 8, 2020

University Utrecht
Institute of Theoretical Physics - Condensed Matter Theory

Acknowledgements

I would like to thank the following people for helping me finalize this Master's project.

I greatly appreciated the help provided by Professor Lizardo Nunes. Before the corona lock-down, I could always drop by his office with any questions, and the weekly check-ins really helped keeping me on track. Afterwards, corona forced us to develop new ways to communicate, and he was still always reachable. He has helped me greatly with feedback, suggesting useful literature, and I am grateful for his dedication and overall help.

I wish to extend my thanks as well to Professor Cristiane de Morais Smith for the proposal of this interesting topic, her incredibly contagious enthusiasm, her clear and calm way of explaining things, the large amount of detailed feedback, and the general care for my progress during these past months.

I would also like to give my appreciation to the following people, namely Rodrigo Ozela for the feedback on my presentations both during the regular Master's course and during this project, and Rodrigo Arouca for tips and explanations on the spin-fermion Hubbard model.

Further, I would like to thank two of my fellow master students. I am very thankful to Johannes Reiher for studying together in a calm and focused manner, as well as the interesting conversations in coffee and lunch breaks, and all other fun activities. I am also grateful to Andri Stylianou for being present for testing software, a trial presentation and my final talk, for nice, comforting conversations throughout the year, and just generally being there and staying in touch.

Finally, I would also like to thank my mother Birgit Schönecker for emotional support and the occasional push to sit back down and get things done.

Abstract

In this work, the influence of nonmagnetic impurities in the form of zinc ions on the superconducting state of lanthanum strontium copper oxide (LSCO) will be studied. The superconducting system is described by the spin-fermion Hubbard model and its superconductivity characterised by the critical temperature. The replacement of copper by zinc atoms changes the superconducting coupling and the kinetic energy of the itinerant holes. This dependence on the zinc concentrations is found from a fit to experimental results and explained in the picture of an excluded area around each zinc impurity.

Lanthanum copper oxide consists of layers of copper-oxygen planes and charge reservoirs. Superconductivity arises when sufficiently many lanthanum ions are replaced by strontium ions in the charge reservoirs, adding itinerant holes to the copper-oxygen planes. These itinerant holes on the oxygen ions and the original localized holes on the copper sites are described by the spin-fermion Hubbard model, which consists of a Hubbard Hamiltonian for the itinerant holes, an antiferromagnetic Heisenberg Hamiltonian for the localized holes and a Kondo interaction Hamiltonian between the two types of holes.

As a result of the replacement of copper with zinc, the critical temperature of the superconducting phase is reduced until the superconducting state vanishes completely at the critical zinc concentration. The zinc dependence enters the critical temperature via the superconducting coupling, the critical coupling and the system's typical energy scale, all of which depend in the same manner on the zinc doping and the critical zinc concentration. A possible explanation for this dependence and a way to find the critical zinc concentration from the strontium doping level will be given.

Contents

Chapter 1

Introduction

Superconductivity is the fascinating phenomenon of vanishing resistivity and the expulsion of magnetic fields, which occurs in certain materials at low temperatures [1]. A superconductor's perfect conductance allows the transportation of currents without energy loss and resulting heat production. Because of this and the bending of external magnetic fields, superconductors could be used to make very efficient power lines, or magnetic levitating trains [2, 3]. This makes superconducting materials very interesting for everyday appliances. However, the superconductors so far discovered only become superconducting at low temperatures, which means that their usage would require extensive cooling. Though progress has been made in discovering and creating superconductors with higher and higher transition temperatures, room temperature has yet to be reached.

To aid in the search for higher temperature superconducting materials, it is important to understand where the superconductivity comes from, to find what the underlying mechanism is. The first class of superconductors, which were discovered in the 1910's, were metals with transition temperatures of a few Kelvin [4]. The first microscopic theory to describe these metals satisfactorily was proposed by Bardeen, Cooper and Schrieffer in 1957 [5]. However, eventually insulating materials were found to become superconducting upon doping, i.e. under the addition of charge carriers, which had higher critical temperatures than could be accounted for with the metallic theory [6].

These high-temperature superconductors also come in a variety of classes, depending on their composition. The focus of this thesis is on the cuprates, insulating compounds containing copper-oxygen layers separated by other atoms [7]. In these materials, the superconducting phase depends not only on the temperature, but also on the type of atoms between the copper-oxygen planes. A doping process changes these atoms and adds the charge carriers responsible for superconductivity to the copper-oxygen planes. So far, many attempts have been made to describe the behaviour of these high-temperature superconductors, however, no unifying theory describing the underlying mechanism has been found yet. A popular approach to discovering the origin of high-temperature superconductivity is the investigation into the destruction of it by the inclusion of impurities. The hope is that from determining how the superconductivity disappears, its emergence will be uncov-

ered. This understanding could help find stronger superconductors for even higher temperatures.

The goal of the research behind this thesis is to describe the influence of nonmagnetic zinc impurities on the superconducting phase of the strontium doped cuprate $La_{2-x}Sr_xCuO_4$, to gain insight into the mechanism underlying high-temperature superconductivity.

The structure of this report is the following. In the first chapter a general introduction to both conventional and high-temperature superconductivity will be given. For conventional superconductivity, the focus will be on London theory and Landau-Ginzburg theory for a macroscopic description and Bardeen-Cooper-Schrieffer theory from a quantum field theory approach for a microscopic description. The high-temperature superconductivity will be discussed based on the description of the structure and the behaviour of the cuprate superconductors as found from experiments. A short overview of some wide-spread models for these compounds will also be given.
In the second chapter, the doping of the cuprate La_2CuO_4 will be described. In the first section of this chapter, the effect of nonmagnetic impurity doping, in the particular case of zinc, on the antiferromagnetic ground state and the critical Néel temperature will be investigated. The system is modelled by a generalized nonlinear σ model and the doping included using percolation theory. In the second part of this chapter, the critical temperature for the superconducting phase as a function of strontium or hole doping will be featured. This will be done using the spin-fermion Hubbard model.
In the third chapter, the effect on the superconducting critical temperature of both types of doping combined will be studied. The combination of the two dopant types according to the previous chapter will be considered, a comparison to experimental data will be made and possible theoretical explanations will be discussed.

Chapter 2

Background on superconductivity

2.1 Conventional superconductivity

The mechanism of superconductivity was first discovered in 1911 by a student of Kamerlingh-Onnes, who found that the resistivity in mercury vanishes abruptly below a certain temperature, which is depicted in figure 2.1 [4]. Afterwards, many more materials with a superconducting phase were discovered [8]. The critical temperature T_c at which their resistivity drops to zero was the first defining quantity of superconductivity.

Roughly twenty years later, Meissner and Ochsenfeld discovered that a superconductor, when placed in an external magnetic field, expels the field [9]. That is, the external field is bent around the superconductor, but does not penetrate inside it. This was afterwards called the Meissner(-Ochsenfeld) effect and it makes the superconductor a perfect diamagnet. However, there is a maximum magnetic field, the critical field H_c, above which superconductivity disappears [1]. To be more precise, there are two ways in which the superconductivity can disappear for increasing magnetic field, leading to two types of superconductors:

- type I superconductors have a clear critical magnetic field above which the superconductivity abruptly disappears. This field is small, on the order of tenths of a Tesla. Pure metals are the largest group of materials in this type.

- type II superconductors do not have a discontinuity in the resistivity at a certain critical field value, but rather loose their superconductivity gradually between two critical field values, H_{c1} and H_{c2}. The upper limit H_{c2} is usually of the order of tens or hundreds of Tesla.

Another way to break the superconducting state besides temperature or magnetic field strength is through a critical current. Often experiments look at both critical field and critical current (see for example [10]).

From further experiments investigating the critical temperature of superconductors, it was discovered that T_c depends on the isotope of a material, in such a way that $T_c \propto {m_a}^{-1/2}$ where m_a is

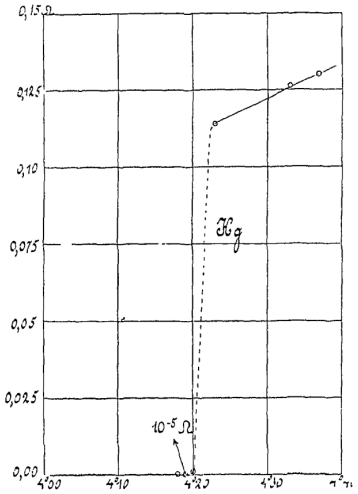

Figure 2.1: Drop in resistivity of mercury as found by Kamerlingh Onnes and his student [4].

the atomic mass [11]. This led to the believe that not just the electrons matter in superconductivity, but also the ionic background lattice. Another effect adding to this believe was sound attenuation, also known as phonon mode softening. In this effect, the coupling between electrons and phonons leads to a decrease in the phonon's frequency and a widening of phonon peaks dependent on temperature as found from Rayman scattering experiments [12, 13].

2.1.1 London and Ginzburg-Landau theory

After the discovery of the superconducting phase, several attempts at describing superconductivity theoretically were made. The most famous, macroscopic descriptions are the London theory from the 1930's and Ginzburg-Landau theory from the 1950's [1].

London's theory has as focus not to describe a perfect conductor, but a perfect diamagnet, that is a material with magnetic induction $\mathbf{B} = 0$ [14]. The theory is based on the assumption that in a superconductor the electrons are accelerated by an external electrical field without dissipation (vanishing resistivity). Starting from Newton's equation for an electric force

$$m^* \frac{\mathrm{d}\mathbf{v}_s}{\mathrm{d}t} = -e^* \mathbf{E}, \tag{2.1}$$

where $\mathbf{v}_s$ is the speed of the supercurrent density $\mathbf{j}_s = -e^* n_s \mathbf{v}_s$, and m^* and e^* are the effective mass and charge, respectively, of the superconducting particles, the first London equation is

$$\frac{\mathrm{d}\mathbf{j}_s}{\mathrm{d}t} = \frac{e^{*2} n_s}{m^*} \mathbf{E}. \tag{2.2}$$

Here n_s is the number density of the superconducting particles. Applying a rotational on both sides of this equation and using Faraday's law $\boldsymbol{\nabla} \times \mathbf{E} = -\partial \mathbf{B}/\partial t$ leads to the second London equation

$$\boldsymbol{\nabla} \times \mathbf{j}_s + \frac{e^{*2} n_s}{m^*} \mathbf{B} = 0. \tag{2.3}$$

To be precise, the time-derivative is actually zero and the left-hand side of the above equation should just be equal to a constant. However, London postulated that the constant should be zero. This also follows from minimizing the total energy.

With Ampère's law for a static electric field, $\boldsymbol{\nabla} \times \mathbf{B} = \mu_0 \mathbf{j}_s$, the second London equation can be rewritten, after some algebra and using that $\boldsymbol{\nabla} \cdot \mathbf{B} = 0$, as [1]

$$\boldsymbol{\nabla} \times (\boldsymbol{\nabla} \times \mathbf{B}) = \mu_0 \boldsymbol{\nabla} \times \mathbf{j}_s, \tag{2.4}$$

$$\boldsymbol{\nabla}(\boldsymbol{\nabla} \cdot \mathbf{B}) - \nabla^2 \mathbf{B} = -\mu_0 \frac{e^{*2} n_s}{m^*} \mathbf{B}, \tag{2.5}$$

$$\nabla^2 \mathbf{B} - \frac{1}{\lambda_L^2} \mathbf{B} = 0, \tag{2.6}$$

where $\lambda_L^2 = m^*/(\mu_0 n_s e^{*2})$ is the (London) penetration depth. This indicates that the induced field is not absolutely expelled from the superconductor, but rather disappears over a finite length scale.

An important difference between a perfect conductor and a superconductor is in the way the induced field is canceled [1]. Both would expel a magnetic field, see figure 2.2b. However, if the magnetic field is turned on in the normal state of the materials and the temperature is lowered, the perfect conductor will no longer expel the field, see figure 2.2a. This difference shows that while a perfect conductor, obeying only Lenz's law, retains the information of its past, the superconductor always has $\mathbf{B} = 0$, independent of when the external field was turned on.

Another important theory is the Ginzburg-Landau theory, which combines electromagnetism with thermodynamics and is built on the Landau theory for phase transitions. The goal is to describe the behaviour of an order parameter ψ, that vanishes in the normal phase, but becomes non-zero in the superconducting phase. The usual Landau free energy for a spatially fluctuating order parameter is given by

$$F = F_0 + \int \left(\alpha(T) |\psi|^2 + \frac{\beta}{2} |\psi|^4 + \gamma |\boldsymbol{\nabla} \psi|^2 \right) \mathrm{d}^3 \mathbf{r} \,. \tag{2.7}$$

The generalization of the Landau free energy is done by including an electromagnetic potential field $\mathbf{A}$ in a gauge invariant way, leading to

$$F_s = F_n + \int \left(\alpha |\psi|^2 + \frac{\beta}{2} |\psi|^4 + \frac{1}{2m^*} |(-i\hbar \boldsymbol{\nabla} - e^* \mathbf{A}) \, \psi|^2 + \frac{|\boldsymbol{\nabla} \times \mathbf{A}|^2}{2\mu_0} \right) \mathrm{d}^3 \mathbf{r} \,, \tag{2.8}$$

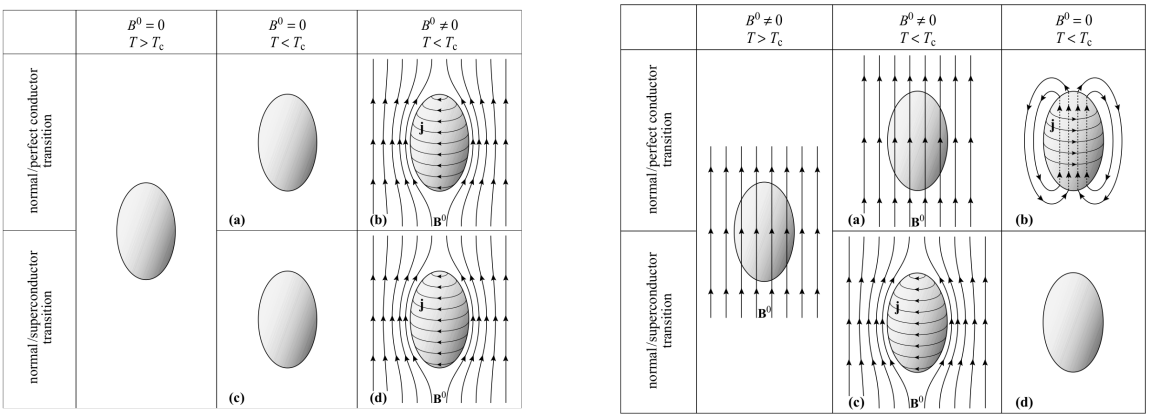

(a) (b)

Figure 2.2: The difference in behavior between a perfect conductor and a superconductor. (2.2a) The magnetic field is turned on in the low temperature phases and gets repelled from both materials. (2.2b) The magnetic field is turned on before the temperature is lowered and switched off in the low temperature phases, where the perfect conductor retains the field, but the superconductor still expels it.

where m^* is again the effective mass and e^* the effective charge, equal to twice the electron charge. From minimizing the free energy with respect to the order parameter ψ and the field $\mathbf{A}$, one can find the Ginzburg-Landau equations:

$$\alpha\psi + \beta|\psi|^2\psi + \frac{1}{2m^*}\left(-i\hbar\boldsymbol{\nabla} - e^*\mathbf{A}\right)^2\psi = 0, \tag{2.9}$$

$$\frac{\hbar e^*}{2im^*}(\psi^*\boldsymbol{\nabla}\psi - \psi\boldsymbol{\nabla}\psi^*) - \frac{e^{*2}}{m^*}\mathbf{A}|\psi|^2 = \frac{1}{\mu_0}\boldsymbol{\nabla}\times\mathbf{B}. \tag{2.10}$$

There are no general solutions to these equations. However, by studying some limiting cases, two important length scales can be determined. The first is again the London penetration depth, $\lambda_L^2 = m^*/(\mu_0 n_s^* e^{*2})$ with $n_s^* = |\alpha|/\beta$. The other length scale found from Ginzburg-Landau theory is the coherence length $\xi^2 = \hbar^2/2m^*|\alpha|$, which gives the scale of spatial fluctuations. The ratio between these two length scales

$$\kappa = \frac{\lambda_L}{\xi} = \frac{m^*}{\hbar e^*}\sqrt{\frac{2\beta}{\mu_0}} \tag{2.11}$$

is called the Ginzburg parameter and determines the type of superconductor. For $\kappa \ll 1$ ($\lambda_L \ll \xi$), the material is a type I, for $\kappa \gg 1$ ($\xi \gg \lambda_L$) a type II superconductor.

As mentioned before, the type II superconductors have two critical magnetic fields, between which the field can partially penetrate the material. This intermediate phase is called the Shubnikov phase and the field enters the material here as a lattice of flux tubes. These fluxes are

quantized by a flux quantum

$$\phi_0 = \frac{h}{e^*} = \frac{h}{2e}, \tag{2.12}$$

which follows readily from the Ginzburg-Landau theory. To see this, consider splitting the order parameter into an amplitude and a complex phase

$$\psi = |\psi| e^{i\chi} \tag{2.13}$$

leading to a supercurrent density

$$\begin{aligned} \mathbf{j}_s &= \frac{\hbar e^*}{2im^*}(\psi^* \boldsymbol{\nabla}\psi - \psi \boldsymbol{\nabla}\psi^*) - \frac{e^{*2}}{m^*}\mathbf{A}|\psi|^2 \\ &= \frac{e^*\hbar}{m^*}|\psi|^2 \boldsymbol{\nabla}\chi - \frac{e^{*2}}{m^*}|\psi|^2 \mathbf{A}. \end{aligned} \tag{2.14}$$

Since the current far from the flux tubes vanishes, the phase term equals the potential field term. Integrating over a closed loop leads to

$$\begin{aligned} \oint_C \boldsymbol{\nabla}\chi \cdot \mathrm{d}\mathbf{r} = \frac{e^*}{\hbar}\oint_C \mathbf{A}\cdot \mathrm{d}\mathbf{r} &= \frac{e^*}{\hbar}\int_\Sigma (\boldsymbol{\nabla}\times\mathbf{A})\cdot \mathrm{d}\sigma \\ &= \frac{e^*}{\hbar}\int_\Sigma \mathbf{B}\cdot \mathrm{d}\sigma \equiv \frac{e^*}{\hbar}\phi_c, \end{aligned} \tag{2.15}$$

where ϕ_c is the magnetic flux. Since the order parameter is uniform, i.e. its value should be the same after a closed loop, the flux has to be an integer multiple of 2π, so that

$$\phi_c = n\frac{\hbar 2\pi}{e^*} = n\frac{h}{2e} \equiv n\phi_0, \tag{2.16}$$

giving rise to the quantization of the magnetic flux.

To summarize, the main characteristics of superconductors are the resistivity drop and the exclution of magnetic fields, up to a critical field, which leads to the different types of superconductors. The behaviour of superconductors in magnetic fields can be described by the London theory or by the Ginzburg-Landau theory. However, these are macroscopic theories and do not give an explanation of the underlying mechanism responsible for superconductivity yet.

2.1.2 BCS theory

The fundamental description of the microscopic origin of superconductivity came a few years after the development of Ginzburg-Landau theory from Bardeen, Cooper and Schrieffer [5]. It was known from the isotope effect and the sound attenuation that phonons were involved in the appearance of superconductivity. From the flux quantization it was known that the effective charge carriers had twice the electron charge. These findings led to the idea that the phonons could be responsible for

an attractive interaction between two electrons. Intuitively, this works as follows [1]: one electron moving through the positively charged lattice causes a slight displacement of the surrounding ions. After the electron has passed through, a slightly positively charged area remains behind, attracting another electron. This only works for electrons at the Fermi surface with a low momentum, i.e. at low temperatures. However, at low temperatures, even a small attraction is sufficient to cause a superconductive state.

Such a pair of electrons that have opposite momentum and spin forms an energetically favourable bound state called a Cooper pair. Only electrons with a kinetic energy ε_k in the range $\varepsilon_F - \hbar\omega_D < \varepsilon_k < \varepsilon_F + \hbar\omega_D$, where ω_D is the Debye frequency and $\hbar\omega_D$ the maximum phonon energy, are available to form Cooper pairs. Favouring the formation of these Cooper pairs energetically, more and more electrons pair up and the Cooper pairs form a new many-body groundstate similar to a Bose-Einstein condensate [15]. In this subsection, the physics of this system will be described using a field theory approach to the original BCS model.

The action for the superconducting electrons in this approach is given by

$$\begin{aligned}\mathcal{S}\left[\psi^\dagger,\psi\right] = \sum_{\sigma=\uparrow,\downarrow}\int_0^{\hbar\beta}\mathrm{d}\tau\int\mathrm{d}\mathbf{x}\,\psi_\sigma^\dagger(\mathbf{x},\tau)\left[\hbar\frac{\partial}{\partial\tau}-\frac{\hbar^2\nabla^2}{2m}-\mu\right]\psi_\sigma(\mathbf{x},\tau)\\ +\int_0^{\hbar\beta}\mathrm{d}\tau\int\mathrm{d}\mathbf{x}\,V_0\psi_\uparrow^\dagger(\mathbf{x},\tau)\psi_\downarrow^\dagger(\mathbf{x},\tau)\psi_\downarrow(\mathbf{x},\tau)\psi_\uparrow(\mathbf{x},\tau),\end{aligned} \tag{2.17}$$

where $\psi_\sigma(\mathbf{x},\tau)$ and $\psi_\sigma^\dagger(\mathbf{x},\tau)$ are the annihilation and creation field operators of electrons with spin σ, m is the electron mass, μ is the chemical potential, and V_0 is an attractive interaction potential between pairs of electrons of opposite spin [15]. The interaction term couples two fermionic fields with different spins, as any term with a product of annihilation fields with the same spin would vanish, due to the fermionic nature of the electrons [7]. The corresponding partition function is given by

$$\mathcal{Z} = \frac{1}{\mathcal{Z}_0}\int\mathcal{D}\psi_\sigma^\dagger\mathcal{D}\psi_\sigma e^{iS\left[\psi^\dagger,\psi\right]/\hbar}, \tag{2.18}$$

where $\mathcal{Z}_0$ is the non-interacting partition function. To be able to work with this action, the quartic interaction term needs to be dealt with using a Hubbard-Stratonovich transformation to a complex field $\eta(\mathbf{x},\tau)$ such that

$$\mathcal{Z} = \frac{1}{\mathcal{Z}_\eta\mathcal{Z}_0}\int\mathcal{D}\psi_\sigma^\dagger\mathcal{D}\psi_\sigma\mathcal{D}\eta^\dagger\mathcal{D}\eta e^{\frac{i}{\hbar}\left(S\left[\psi^\dagger,\psi\right]-\int_0^{\hbar\beta}\mathrm{d}\tau\int\mathrm{d}\mathbf{x}\frac{1}{V_0}\eta^\dagger\eta\right)}. \tag{2.19}$$

The quartic interaction term in the fermionic fields can then be removed by shifting the functional integral over η to

$$\eta \to \eta + V_0\psi_\uparrow\psi_\downarrow, \tag{2.20}$$

$$\eta^\dagger \to \eta^\dagger + V_0\psi_\downarrow^\dagger\psi_\uparrow^\dagger, \tag{2.21}$$

which does not change the functional integration measure. The resulting action is then

$$\begin{aligned}\mathcal{S}\left[\eta^\dagger,\eta,\psi^\dagger,\psi\right] = &-\int_0^{\hbar\beta}\mathrm{d}\tau\int\mathrm{d}\mathbf{x}\,\frac{|\eta(\mathbf{x},\tau)|^2}{V_0}\\ &+\sum_{\sigma=\uparrow,\downarrow}\int_0^{\hbar\beta}\mathrm{d}\tau\int\mathrm{d}\mathbf{x}\,\psi_\sigma^\dagger(\mathbf{x},\tau)\left(\hbar\frac{\partial}{\partial\tau}-\frac{\hbar^2\nabla^2}{2m}-\mu\right)\psi_\sigma(\mathbf{x},\tau)\\ &+\int_0^{\hbar\beta}\mathrm{d}\tau\int\mathrm{d}\mathbf{x}\left\{\psi_\uparrow^\dagger(\mathbf{x},\tau)\psi_\downarrow^\dagger(\mathbf{x},\tau)\eta(\mathbf{x},\tau)+\eta^\dagger(\mathbf{x},\tau)\psi_\downarrow(\mathbf{x},\tau)\psi_\uparrow(\mathbf{x},\tau)\right\}.\end{aligned} \tag{2.22}$$

By varying the action with respect to the complex fields η and $\eta^\dagger$, the field equations

$$\eta = V_0\psi_\downarrow\psi_\uparrow, \tag{2.23}$$

$$\eta^\dagger = V_0\psi_\uparrow^\dagger\psi_\downarrow^\dagger \tag{2.24}$$

are obtained, indicating that the complex auxiliary field η is the Cooper pair field. Its vacuum expectation value $\langle 0|\eta|0\rangle = V_0\langle 0|\psi_\downarrow\psi_\uparrow|0\rangle$ gives the Cooper pair density in the ground state. Because of this, it can serve as an order parameter for the superconducting phase.

To evaluate the action of equation (2.22), which is now only quadratic in the fermionic fields, it is useful to switch to the so-called Nambu fermion fields $\Phi^\dagger = \begin{pmatrix}\psi_\downarrow^\dagger & \psi_\uparrow\end{pmatrix}$, so that the action can be written in a matrix form

$$\begin{aligned}\mathcal{S}\left[\eta^\dagger,\eta,\psi^\dagger,\psi\right] = &-\int_0^{\hbar\beta}\mathrm{d}\tau\int\mathrm{d}\mathbf{x}\,\frac{|\eta(\mathbf{x},\tau)|^2}{V_0}\\ &+\int_0^{\hbar\beta}\mathrm{d}\tau\int\mathrm{d}\mathbf{x}\,\Phi^\dagger\mathbf{A}\Phi,\end{aligned} \tag{2.25}$$

where $\mathbf{A}$ is given by

$$\mathbf{A} = \begin{pmatrix}\xi(\mathbf{k})+i\hbar\omega_n & \eta\\ \eta^\dagger & \xi(\mathbf{k})-i\hbar\omega_n\end{pmatrix} \tag{2.26}$$

in momentum space, with $\xi(\mathbf{k}) = \hbar^2\mathbf{k}^2/(2m)-\mu$ the kinetic energy of the electrons with respect to the Fermi level and ω_n the fermionic Matsubara frequency [7]. The component $\mathbf{A}_{22}$ obtains a minus sign, because of the interchange of the fermion fields $\psi_\downarrow^\dagger$ and $\psi_\downarrow$ in the Nambu vector notation. Now the fermionic fields in the partition function can be integrated out in the partition function of equation (2.19) leading to an effective action in terms of the Cooper pair field

$$\mathcal{S}_{eff}\left[\eta^\dagger,\eta\right] = -\int_0^{\hbar\beta}\mathrm{d}\tau\int\mathrm{d}\mathbf{x}\frac{|\eta(\mathbf{x},\tau)|^2}{V_0} - i\ln\det\left[\frac{\mathbf{A}[\eta]}{\mathbf{A}[0]}\right], \tag{2.27}$$

where $\det\mathbf{A}[\eta] = \xi^2+(\hbar\omega_n)^2-|\eta|^2$, so that, in real space, the effective action for the Cooper pair field becomes

$$\mathcal{S}_{eff}\left[\eta^\dagger,\eta\right] = -\int_0^{\hbar\beta}\mathrm{d}\tau\int\mathrm{d}\mathbf{x}\frac{|\eta(\mathbf{x},\tau)|^2}{V_0} - i\,\mathrm{Tr}\ln\left[1-\frac{|\eta|^2}{-\partial_\tau^2+\left(-\frac{\hbar^2\nabla^2}{2m}-\mu\right)^2}\right]. \tag{2.28}$$

From this effective action, the effective potential as a function of the order parameter of superconductivity, $\Delta = \langle 0|\eta|0\rangle$, can be extracted [7]. It is given by

$$V_{eff}(|\Delta|,T) = \frac{|\Delta|^2}{V_0} - k_B T \int \frac{\mathrm{d}^3\mathbf{k}}{(2\pi)^3} \sum_{n=-\infty}^{\infty} \left\{ \ln\left[1 + \frac{|\Delta|^2}{\hbar^2\omega_n^2 + \xi(\mathbf{k})^2} \right] \right\}. \tag{2.29}$$

Since the only electron states contributing to the momentum integral are the ones in the region of $\hbar\omega_D$ around the Fermi surface, the integral can be rewritten as

$$\int \frac{\mathrm{d}^3\mathbf{k}}{(2\pi)^3} = \int_{-\hbar\omega_D}^{\hbar\omega_D} \mathrm{d}\xi\, N_{FD}(\xi) \simeq N_{FD}(E_F) \int_{-\hbar\omega_D}^{\hbar\omega_D} \mathrm{d}\xi\,, \tag{2.30}$$

where $N_{FD}(\xi) = 1/(\exp(\beta\xi)+1)$ is the Fermi-Dirac distribution or density of states at the energy level ξ and it can be taken to be roughly equal to the distribution at the Fermi energy in the domain of the integral, because $\hbar\omega_D \ll E_F$.

To find the superconducting and normal phases of the system, one needs to find the stable equilibrium points of the effective potential [7]. These points are the solutions to

$$\frac{\partial}{\partial|\Delta|} V_{eff}(|\Delta|,T) = 0, \tag{2.31}$$

$$\frac{\partial^2}{\partial|\Delta|^2} V_{eff}(|\Delta|,T) > 0. \tag{2.32}$$

The condition for the vanishing first derivative results in

$$2|\Delta| \left\{ \frac{1}{V_0} - k_B T N_{FD}(E_F) \int_{-\hbar\omega_D}^{\hbar\omega_D} \mathrm{d}\xi \sum_{n=-\infty}^{\infty} \left[\frac{1}{\hbar^2\omega_n^2 + \xi^2 + |\Delta|^2} \right] \right\} = 0, \tag{2.33}$$

where the Matsubara sum can be carried out using $\sum 1/\left[a^2 + (n+\frac{1}{2})^2\right] = {}^{\pi}/_{a} \tanh(\pi a)$ leading to

$$2|\Delta| \left\{ \frac{1}{V_0} - N_{FD}(E_F) \int_0^{\hbar\omega_D} \mathrm{d}\xi\, \frac{\tanh\left(\frac{\sqrt{\xi^2+|\Delta|^2}}{2T} \right)}{\sqrt{\xi^2+|\Delta|^2}} \right\} = 0. \tag{2.34}$$

In the superconducting phase $|\Delta| \neq 0$ and the term between brackets in the above equation must vanish, resulting in the gap equation

$$1 = V_0 N_{FD}(E_F) \int_0^{\hbar\omega_D} \mathrm{d}\xi\, \frac{\tanh\left(\frac{\sqrt{\xi^2+|\Delta|^2}}{2k_B T} \right)}{\sqrt{\xi^2+|\Delta|^2}}. \tag{2.35}$$

In the limit $T \to T_c$, the order parameter vanishes and the energy integral can be performed by an integration by parts ([16])

$$\int_0^B \frac{\mathrm{d}z}{z} \tanh z = \ln z \tanh z \Big|_0^B - \int_0^B \mathrm{d}z \ln z \operatorname{sech}^2 z. \tag{2.36}$$

For $z = \frac{\xi}{2k_B T_c}$, the upper bound $B = \frac{\hbar\omega_D}{2k_B T}$ is very large, because $\hbar\omega_D \gg k_B T$ at low temperatures, and the gap equation gives approximately

$$1 \approx V_0 N_{FD}(E_F) \left(\ln \frac{\hbar\omega_D}{2k_B T_c} - \int_0^\infty \mathrm{d}z \ln z \operatorname{sech}^2 z \right), \tag{2.37}$$

where the remaining integral is given by

$$\int_0^\infty \mathrm{d}z \ln z \operatorname{sech}^2 z = -\ln \frac{4e^\gamma}{\pi}, \tag{2.38}$$

so that, after solving for the critical temperature, one finds

$$k_B T_c = \frac{2e^\gamma}{\pi} \hbar\omega_D e^{1/N_{FD}(E_F)V_0} \approx 1.13 \hbar\omega_D e^{1/N_{FD}(E_F)V_0}. \tag{2.39}$$

Note here that T_c is small compared to the phonon energy due to the exponential factor and the small attractive interaction. Also, the direct dependence of the temperature on the phonon energy explains the isotope effect, as the Debye frequency goes exactly as $M^{-1/2}$.

In the opposite limit, that is for $T \to 0$, the gap equation reduces to

$$1 = V_0 N_{FD}(E_F) \int_0^{\hbar\omega_D} \frac{\mathrm{d}\xi}{\sqrt{\Delta^2 + \xi^2}} \approx V_0 N_{FD}(E_F) \ln \frac{2\hbar\omega_D}{\Delta}, \tag{2.40}$$

where the last equation holds only the leading term for $\hbar\omega_D/\Delta \gg 1$ [16]. This leads to the maximum value of the energy gap at zero temperature

$$\Delta_0 = 2\hbar\omega_D e^{1/V_0 N_{FD}(E_F)}. \tag{2.41}$$

Just like the critical temperature, the maximum energy gap depends on the exponent of $V_0 N_{FD}(E_F)$. When forming the ratio of these two,

$$\frac{\Delta_0}{k_B T_c} = \pi e^{-\gamma} \approx 1.76, \tag{2.42}$$

the dependence on the material cancels and a universal constant is recovered.

The full temperature dependence of the gap can be found numerically and is given by

$$\Delta(T) \approx \Delta_0 - (2\pi\Delta_0 k_B T)^{\frac{1}{2}} e^{-\Delta_0/k_B T} \tag{2.43}$$

for $T \ll T_c$, and

$$\Delta(T) \approx 3.06 k_B T_c \left(1 - \frac{T}{T_c}\right)^{\frac{1}{2}} \tag{2.44}$$

for $T_c - T \ll T_c$ [16]. See figure 2.3 for the energy gap as a function of the temperature.

A second experimental finding that BCS theory explains is the behaviour of the specific heat as a function of the temperature [5]. The specific heat measures the amount of energy put into a system that is used to increase the system's temperature. For most materials, a part of the specific heat comes from the phonons and the remainder from the electrons [17]. In the superconducting phase, the electronic specific heat varies exponentially with the temperature, while at the critical temperature, the specific heat discontinuously drops to the usual normal state electronic specific heat and increases linearly with temperature, see also figure 2.4.

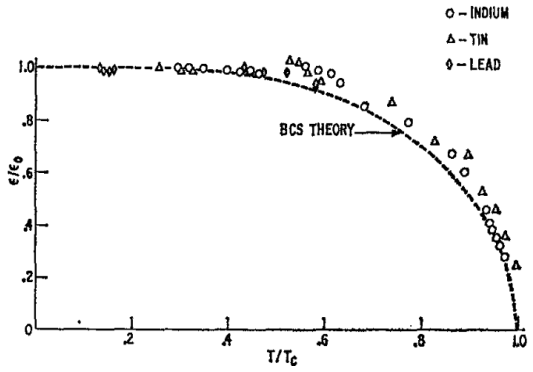

Figure 2.3: Temperature dependence of the gap energy as described by BCS theory and found from experiments [18].

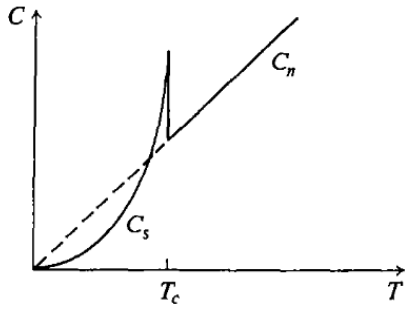

Figure 2.4: Schematic representation of the specific heat as a function of temperature, exhibiting an exponential dependence in the superconducting phase and a discontinuity at the critical temperature [16].

The BCS theory predicts a temperature-depedence of the specific heat near zero temperature as

$$C_T \approx 8.5\,\alpha\,T_c\,e^{-1.44\,T_c/T}\,, \tag{2.45}$$

where $\alpha = \frac{2}{3}\pi^2 k_B^2 N_{FD}(\varepsilon_F)$ [5]. The values for the constants 8.5 and -1.44 in this relation come very close to experimental results for several different materials [19], indicating that the exponential behaviour of the specific heat stems indeed from a gap in the energy. With their theory, Bardeen, Cooper and Schrieffer also recovered the jump in the specific heat at the critical temperature, which shows that the phase transition from the normal to the superconducting state is a second order transition.

2.2 High-T$_c$ superconductivity in cuprates

In 1957, the first superconductor with a high critical temperature of $T_c \approx 30$ K was found by Müller and Bednorz [6]. Similar to the low-temperature or conventional superconductors, the high-T_c materials have a drop in the resistivity [1]. However, these superconductors show some prominent differences with the conventional metallic superconductors. For example, most of them are insulators in the undoped normal phase instead of conducting metals described by Fermi liquid theory. Also, the isotope effect on the critical temperature is very small compared to the conventional superconductors' effect [20] and magnetic interactions play an important role, that is the conducting phase can coexist with magnetic fluctuations or even a magnetically ordered phase [21, 22].

Because of these differences and the high critical temperature, it is believed that these materials do not become superconducting mainly through phonon-coupled Cooper pairs and that they can therefore no longer be described by the BCS theory [7]. No general theory has been found to describe all types of high-T_c superconductors, but for certain materials some models were made. The focus of this thesis will be on high-temperature superconducting cuprates, and more specifically $La_{2-x}Sr_xCuO_4$. In this section, the undoped cuprates' crystal structure, an outline of the behaviour of cuprates when they become hole-doped and an indication of the theoretical description by the three-band and some one-band models will be given. In principle, cuprates can also become superconducting with electron doping [22], though this will not be further discussed here.

2.2.1 Cuprate lattice structure and experimental features

In general, the structure of the high temperature superconducting cuprates is the following. The cuprates consist of copper-oxygen layers separated by spacer or charge reservoir layers as can be seen in figure 2.5(a) [7]. The superconductivity of these materials is believed to originate in the Cu-O_2 layers [23]. The number of the Cu-O_2 planes between each spacer layer can vary and affects the critical temperature. In $HgBa_2Ca_{n-1}Cu_nO_{2n+2+\delta}$, for example, the critical temperature increases from 98 K for $n = 1$ plane, over 128 K for $n = 2$ up to 135 K for $n = 3$ copper-oxygen planes

[24]. Another well-studied example is the family of $Bi_2Sr_2Ca_{n-1}Cu_nO_{2n+4+\delta}$, where the critical temperature also increases with increasing n [25]. The compound of interest here, $La_{2-x}Sr_xCuO_4$, has a single copper-oxygen plane between the charge reservoirs.

In the undoped system La_2CuO_4, the lanthanum is ionized to La^{3+} and the oxygen to O^{2-} [7]. However, for charge neutrality each copper atom releases two electrons from the $4s$ and the $3d$ shells, which leaves a vacancy in the latter, so that the outer shell is $3d^9$ instead of the filled $3d^{10}$. In the picture of holes this vacancy can be described as one effective spin-$\frac{1}{2}$ particle at each copper site [26]. Due to strong interactions, the undoped system is antiferromagnetically ordered at low temperature and even arranges into the Néel state below the critical temperature T_N [22]. The copper-oxygen lattices of the undoped material as depicted in figure 2.5(b) can therefore be described by a two-dimensional antiferromagnetic Heisenberg model [7].

Figure 2.5: Schematic representation of the structure of cuprates. (a) The layered structure of cuprates [27]. The two superconducting CuO_2-layers are separated by charge reservoir or spacer layers. Note that La_2CuO_4 would contain only one copper-oxygen layer between the spacer layers. (b) Square lattice of the copper-oxygen plane with copper atoms at the lattice sites (black dots) and oxygen atoms forming the links (grey dots) [7].

The copper-oxygen planes only become superconducting when the spacer layers are doped [7]. In the case of $La_{2-x}Sr_xCuO_4$, the strontium replaces some of the La^{3+} and ionizes into Sr^{2+}, adding more holes to the copper-oxygen planes. It is generally assumed that the holes are located on the oxygen ion links rather than on the copper sites, because the onsite Coulomb repulsion is larger than the gap between the energy levels of the outermost copper and oxygen shells [28]. With an increasing surplus of holes, the low-temperature Néel state gets destroyed and the system eventually transitions into a superconducting phase [29, 22], as can be seen in figure 2.6. The superconducting phase begins at zero temperature for some critical doping level $x_{sc,-}$, has an increasing critical temperature $T_c(x)$ up to an optimal doping level x_0, after which the critical temperature decreases again, effectively describing a superconducting dome. Other phases which appear for different doping levels and temperatures are the pseudogap (PG), the spin-glass (SG) and the non-Fermi liquid phase, for example [30].

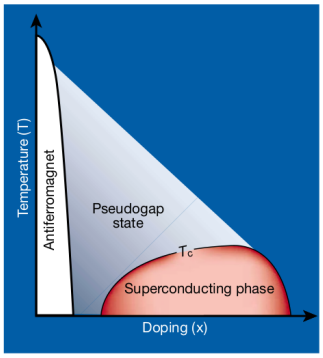

Figure 2.6: Schematic diagram of the phases for superconducting cuprates [31]. At low hole doping and low temperature, the system is in an antiferromagnetic state, at higher doping a superconducting dome appears.

Besides the expanded phase diagram and the before-mentioned smallness of the isotope effect, some other experimental features which characterise the cuprates and set them apart from conventional superconductors are a short coherence length and a momentum dependent order parameter [7]. The coherence length in cuprates is usually of the order of a few nanometer, $\xi \approx 1 - 4$ nm, instead of tens or hundreds of nanometer as for the conventional superconductors, $\xi \approx 50 - 1000$ nm. This means that the coherence length is shorter than the penetration depth and the cuprates are type II superconductors, as described in section 2.1.1.

The momentum dependence of the energy gap for most cuprates was found from angle-resolved photo-emission spectroscopy (ARPES) [7]. ARPES uses the photo-electric effect to emit free electrons and measures their kinetic energy and the angle at which they are emitted [32]. For two-dimensional solids, ARPES gives the density distribution of the electronic excitations (the quasiparticles) over energy and momentum along a certain direction in the reciprocal space. When probing cuprate superconductors, ARPES experiments show a momentum dependence in the order parameter, as opposed to the conventional superconductors, which have a uniform energy gap [7]. The anisotropic order parameter

$$\Delta = \Delta_0 \left[\cos k_x a - \cos k_y a\right], \tag{2.46}$$

where $a \approx 3.8$Å is the lattice spacing between the copper ions, generally has a d-wave symmetry, see figure 2.7. An overview of experiments on the nature of the order parameter in cuprates can be found, for example, in Ref. [33].

To conclude, high-temperature superconducting cuprates have a doping-induced superconductivity originating from the copper-oxygen planes. The superconducting pairs have a small coherence length and give rise to a d-wave type order parameter. A theoretical description of these superconductors should therefore focus on the holes as the charge carriers of the system, and be restrained to the copper-oxygen planes. As examples of such a description, the three-band model and two reduced one-band models will be shortly discussed next.

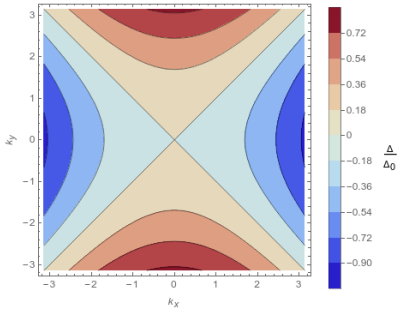

Figure 2.7: The d-wave nature of the order parameter Δ/Δ_0 as a function of momentum.

2.2.2 Three-band model

Besides the assumption that the charge carriers only move in the copper-oxygen planes, the complexity of the superconducting cuprates will also be reduced by considering only the outer shells of the ions. For copper, this is the $d_{x^2-y^2}$ shell and for oxygen these are the p_x and p_y shells, which play a significant role in the superconductivity of cuprates [34]. Since one electron is missing in the $d_{x^2-y^2}$ shell, the system can be represented by a lattice with spin-$\frac{1}{2}$ holes located at the copper ions, into which the doping introduces additional holes [35]. Considering the system with the copper-d and oxygen-p_x and -p_y shells filled as the vacuum state, the Hamiltonian for the holes consists of hopping between copper and oxygen atoms t_{pd}, hopping between oxygen-oxygen neighbours t_p, onsite energies ϵ and onsite-interaction potentials U at the copper and oxygen ions [36, 35, 37]:

$$\begin{aligned} H = &- t_{pd} \sum_{\langle i,j\rangle,\sigma} \left(p^\dagger_{j\sigma} d_{i\sigma} + d^\dagger_{i\sigma} p_{j\sigma} \right) - t_p \sum_{\langle j,j'\rangle,\sigma} \left(p^\dagger_{j\sigma} p_{j'\sigma} + p^\dagger_{j'\sigma} p_{j\sigma} \right) \\ &+ \epsilon_d \sum_{i\sigma} n^d_{i\sigma} + \epsilon_p \sum_{j\sigma} n^p_{j\sigma} + U_d \sum_i n^d_{i\uparrow} n^d_{i\downarrow} \\ &+ U_p \sum_j n^p_{j\uparrow} n^p_{j\downarrow} + U_{dp} \sum_{\langle i,j\rangle,\sigma} n^d_{i\sigma} n^p_{j\sigma}, \end{aligned} \tag{2.47}$$

where the fermionic operators $p^\dagger_j$ create holes at the oxygen sites, $d^\dagger_i$ create holes at the copper sites and $n^z_l = z^\dagger_l z_l$ is the number operator at either oxygen $z = p$, $l = j$ or copper $z = d$, $l = i$ sites. The sums over $\langle l, l'\rangle$ are sums over nearest neighbour copper or oxygen pairs and σ is the spin. See figure 2.8 for an overview of the hoppings and interactions. This Hamiltonian was introduced as an extended Hubbard Hamiltonian [36], but has since become the three-band (Hubbard) Hamiltonian [35].

The three-band model is still difficult to work with, due to the high number of parameters [35]. An attempt to simplify it has been made in the following way. When the system becomes doped in the regime where the onsite-interaction U_d at the copper sites is larger than the energy

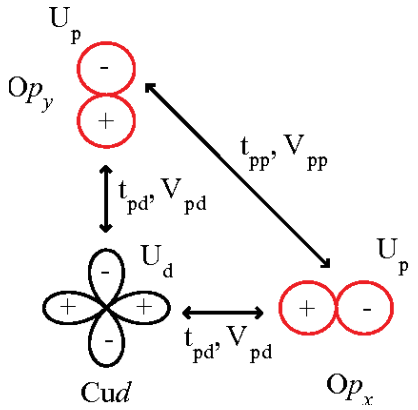

Figure 2.8: Overview of the hopping t_{pd} between the copper and the oxygen sites and t_{pp} between the p-shells of two oxygen sites, the onsite Coulomb repulsions U_d and U_p and the intersite repulsions V_{pd} and V_{pp} (this last one is not included in the Hamiltonian (2.47), while $V_{pd} = U_{dp}$) [38].

difference $\Delta_E = \epsilon_p - \epsilon_d$ (the charge-transfer gap), the added holes will occupy the oxygen sites [36]. Experiments have shown that this is indeed the case in the superconducting cuprates [39]. Since the extra hole on one of the four oxygen ions around the copper atom can couple in a symmetric or antisymmetric way with the original hole of the copper site, the two holes can collectively be described by a spin singlet or triplet state, as described by Zhang and Rice [40]. They further argued that the spin singlet state suffices to describe the system, and the model can be reduced to one with a spin singlet state centered on each copper site, corresponding to an effective model of spins and spin-holes on only the copper lattice. The effective Hamiltonian is given by [41]

$$H = -t \sum_{\langle i,j\rangle,\sigma} c^\dagger_{i\sigma} c_{j\sigma} + U \sum_i n_{i\uparrow} n_{i\downarrow}, \tag{2.48}$$

where $c^\dagger_{i\sigma}$ creates a fermion on the copper sites and U is the onsite repulsive interaction.

An alternative for this reduction of the three-band model to a one-band model is an expansion of the three-band Hubbard model to the so-called $t - J$ Hamiltonian in the strong coupling limit [42]

$$\begin{aligned} H = & -t \sum_{\langle i,j\rangle,\sigma} \left[c^\dagger_{i,\sigma} \left(1 - n_{i,-\sigma}\right) \left(1 - n_{j,-\sigma}\right) c_{j,\sigma} + \text{h.c.} \right] \\ & + J \sum_{\langle i,j\rangle} \left[\mathbf{S}_i \cdot \mathbf{S}_j - \frac{1}{4} n_i n_j \right], \end{aligned} \tag{2.49}$$

with t the hopping energy between the copper sites, whose term preserves the spin and excludes double occupancy of the copper sites, $\mathbf{S}_i$ the spin-1/2 operator and $J = 4t^2/U$ the antiferromagnetic coupling between nearest neighbours. The next term in the expansion is a hopping term

between three sites. Eskes and Eder showed that with the inclusion of this three-site term the $t-J$ model is still relevant in the intermediate coupling regime, which is appropriate for the cuprate superconductors [43].

However, the correctness of the reductions of the three-band model to simpler models is still a matter of discussion. For example, the band models correspond to different types of insulators: the one-band models show the physical behaviour expected for doping a Mott-Hubbard insulator, whereas the actual superconducting cuprates are doped charge-transfer insulators, a fact which is incorporated in the three-band model [41]. The difference between these two lies in the gap existing between bands of same-ion states (Mott insulator) or between bands of the anions and cations (charge-transfer insulator) [44]. Also, it is not clear whether the triplet states between the copper and oxygen holes can really be ignored [45]. In general and especially in the overdoped regime (above the optimal doping level), the oxygen sites become important and can not be simply treated as a pertubation on the copper hole system [46]. In section 3.2 a model which focuses on the oxygen sites will be discussed in detail.

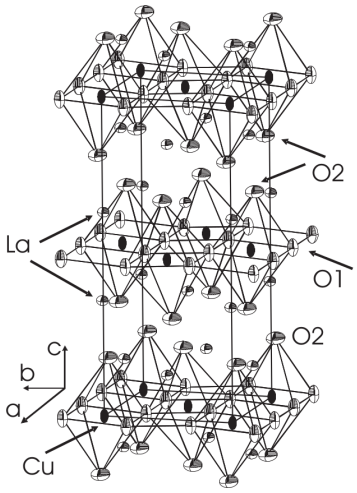

Figure 2.9: Lattice of tilted CuO-octahedra [47].

Another effect that is not included in either the three-band model or the one-band models is the influence of the spacer-layer oxygen atoms on the copper-oxygen planes [48]. In the three-dimensional cuprate lattice, each copper atom is surrounded by six oxygen atoms in a slightly tilted octahedron, see figure 2.9 [49]. Still only the four oxygen atoms in the plane with the copper play a role in the superconducting interactions in the system, as the two so-called apical oxygens in the spacer layers are at a larger distance to the copper atoms and therefore have a much weaker bond [23]. However, the net tilting of the four in-plane oxygens also leads to a Dzyaloshinskii-Moriya (spin-orbit coupling) and a XY (direct exchange) interaction [49], which will be described in more detail in the next chapter when considering the nonlinear σ model.

Chapter 3

Description of doped La_2CuO_4

In this chapter, a theoretical description of the copper-oxygen planes with doping will be given. In the first section, the copper-oxygen planes are doped with nonmagnetic zinc atoms, replacing a fraction of the copper atoms. In the second section, the doping is done by exchanging a fraction of the lanthanum ions in the spacer layers with strontium atoms, which contribute additional holes to the copper-oxygen planes.

In the first section, the goal will be to describe the doping-induced change in the antiferromagnetically ordered state at low temperature by deriving an expression for the Néel temperature using the nonlinear σ model, while the goal of the second section is to find the critical temperature for the superconducting phase as a function of the strontium doping fraction using the Spin-Fermion-Hubbard model. In the next chapter, both types of doping will be combined.

3.1 Nonmagnetic impurity doping

The doping with zinc, resulting in $La_2Cu_{1-z}Zn_zO_4$, is a way to break the magnetic ordering of the undoped insulating compound [49]. The ionized zinc atoms have the same valence as the copper ions, that is, they also release two electrons, but their outer shell is fully filled. This means that there are no free holes on sites where zinc has replaced the copper ions and there is no magnetic interaction between these sites and the spin-1/2 holes on the copper sites. This supresses the antiferromagnetic ordering and destroys superconductivity. There are several other dopants with a similar effect, for example nickel or magnesium [50, 51]. The effect of zinc doping was included in the generalized nonlinear σ model through percolation theory in Ref. [49], which will be explained in more detail below.

The generalized nonlinear σ model follows from an expansion of the antiferromagnetic Heisenberg model for the low temperature state of La_2CuO_2, including anisotropic interactions stemming from the tilted copper-oxygen octahedra, which can be seen in figure 2.9 [49]. However, the model describes again only the copper-oxygen plane, such that the underlying structure is a square lattice. The Hamiltonian for the general nonlinear σ model is derived from the extended Heisenberg

Hamiltonian given by

$$H = H_H + H_{DM} + H_{XY} = \sum_{<I,J>} (J\mathbf{S}_I\mathbf{S}_J + \mathbf{D}_{IJ} \cdot (\mathbf{S}_I \times \mathbf{S}_J) + \mathbf{S}_I\Gamma_{IJ}\mathbf{S}_J) \tag{3.1}$$

where the summation is taken over nearest neighbours on the copper sites. This Hamiltonian has a typical antiferromagnetic exchange energy, but also two terms for the anisotropic interactions [52]. The second term in the above equation gives the Dzyaloshinskii-Moriya (DM) interaction, a spin-orbit coupling, also known as the antisymmetric exchange interaction. The symmetry of the system puts constraints on the orientation of the vector $\mathbf{D}_{IJ}$. For a system with planes as shown in figure 3.1a, the vector components are given by

$$\mathbf{D}_{AB} = \pm\,(0,\, d,\, 0) \tag{3.2}$$
$$\mathbf{D}_{AC} = \pm\,(d,\, 0,\, 0) \tag{3.3}$$

where $\mathbf{D}_{AB}$ is the interaction between neighbours on the x-axis, $\mathbf{D}_{AC}$ the interaction between neighbours on the y-axis and d is the exchange energy of the order $10^{-2}J$ [49]. The DM vectors are perpendicular to the copper bonds and have alternating sign, as can be seen in figure 3.1(b). This means that there are actually two inequivalent neighbours in the sum over nearest neighbours.

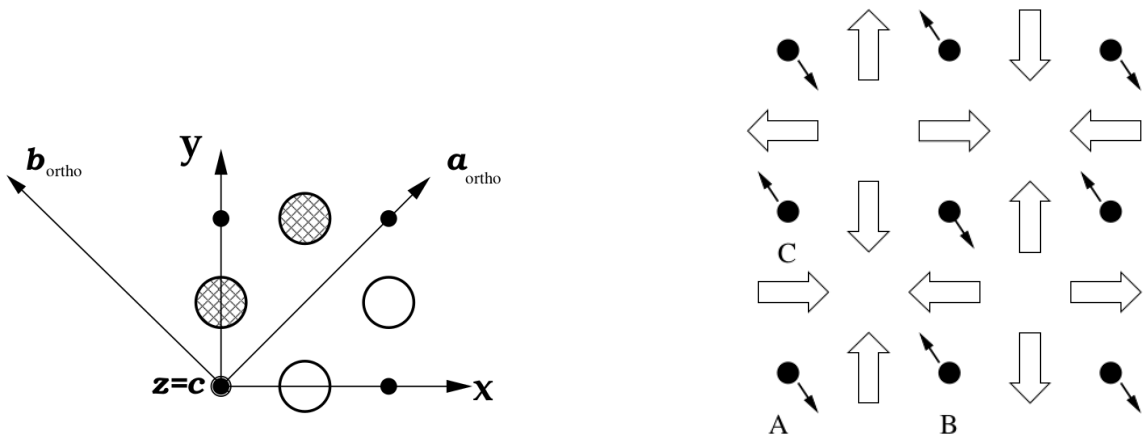

(a) (b)

Figure 3.1: (a) Coordinate system for the copper-oxygen plane. The black dots correspond to the copper atoms, the empty circles represent the oxygen ions titled below the plane, the gray circles the ions above [53]. (b) Schematic representation of the antiferromagnetic spins on the copper sites, represented by the black arrows, and the Dzyaloshinskii-Moriya vectors, indicated by the open arrows [53].

The last term in the Hamiltonian corresponds to the XY interaction, which is a direct-exchange interaction. It is described by

$$\Gamma_{AB} = \begin{pmatrix} \Gamma_1 + \Gamma_2 & 0 & 0 \\ 0 & \Gamma_1 - \Gamma_2 & 0 \\ 0 & 0 & \Gamma_3 \end{pmatrix} \tag{3.4}$$

$$\Gamma_{AC} = \begin{pmatrix} \Gamma_1 - \Gamma_2 & 0 & 0 \\ 0 & \Gamma_1 + \Gamma_2 & 0 \\ 0 & 0 & \Gamma_3 \end{pmatrix}, \tag{3.5}$$

where the components $\Gamma_{1,2,3}$ are of the order of $10^{-4}J$ [49].

The expanded Heisenberg Hamiltonian of equation (3.1) is most useful for the description of low-energy excitations above the Néel ground state. Overall, the system in this region will be antiferromagnetically ordered, with only small long-distance fluctuations [49]. Therefore, the spin of the lattice sites can be decomposed into a staggered or antiferromagnetic component and a uniform or fluctuating component, such that

$$\frac{\mathbf{S}_I}{S} \equiv \mathbf{\Omega}_I \approx (-1)^I \mathbf{n}_I + a\mathbf{l}_I, \tag{3.6}$$

where $\mathbf{\Omega}_I$ is the coherent spin at site I in the copper lattice, a is the lattice spacing, $\mathbf{n}_I$ is the staggered unit spin and $\mathbf{l}_I$ is the perpendicular fluctuation. These last two obey the relations $|\mathbf{n}|^2 = 1$ and $\mathbf{n} \cdot \mathbf{l} = 0$. The nearest-neighbour spins at sites $J = I \pm 1$ can be approximated by an expansion of the staggered component around the spin at site I, while the uniform spin stays roughly the same, i.e.

$$\mathbf{n}_J \approx (-1)^{I\pm1}\mathbf{n}_I - (\mathbf{a} \cdot \nabla)\mathbf{n}_I, \tag{3.7}$$

$$\mathbf{l}_J \approx \mathbf{l}_I. \tag{3.8}$$

Substituting the decomposition (3.6) and the above expansion into the Hamiltonian (3.1) and including doping leads in the long-wavelength or continuum limit ($a^2 \sum_I \to \int \mathrm{d}^2 r$) to

$$H_H = \frac{JS^2K(z)}{2} \int \left[(\nabla \mathbf{n})^2 + 8\mathbf{l}^2\right] \mathrm{d}^2\mathbf{r}\,, \tag{3.9}$$

$$H_{DM} = \frac{4S^2K(z)}{a} \int \left[\mathbf{d}_+ \cdot (\mathbf{n} \times \mathbf{l})\right] \mathrm{d}^2\mathbf{r}\,, \tag{3.10}$$

$$H_{XY} = \frac{2S^2K(z)}{a^2} \int \left[(\Gamma_1 - \Gamma_3)\, n_z^2\right] \mathrm{d}^2\mathbf{r}\,, \tag{3.11}$$

where $\mathbf{d}_+ = (\mathbf{D}_{AB} + \mathbf{D}_{AC})/2$ and in the XY-Hamiltonian the small terms like $\Gamma(\nabla\mathbf{n})^2$ and $\Gamma\mathbf{l}^2$ are neglected. The factor $K(z)$ comes from percolation theory.

Percolation theory is used to include the site-dilution by the doping with zinc atoms. In general, this theory describes clustering in probability distributions over structured systems [54]. In the case of the zinc doping, the clustering can be pictured as follows. The holes at the copper sites interact with each other through a Coulomb repulsion, which forms a bond between one copper site and its four neighbours. When a zinc ion replaces a copper ion, the four interaction bonds are broken and the systems loses its connectivity. See also figure 3.2(a).

In the doped lattice system, the effect of the nonmagnetic zinc ions enters the Hamiltonian as an uncorrelated variable η_I with an expectation value equal to the magnetic concentration, $\langle \eta_I \rangle = p_I$ [49]. The magnetic concentration $p_I = 1$ at a copper site and $p_I = 0$ at a zinc site. This leads to a replacement in the Hamiltonian of $\mathbf{\Omega}_I \cdot \mathbf{\Omega}_J \to p_I p_J \mathbf{\Omega}_I \cdot \mathbf{\Omega}_J$.

Above a critical or limiting concentration p_c, the system forms an infinite cluster, where a connection between two opposite sides of the system could be made via the interaction bonds [54], see figure 3.2(b). However, as more zinc is doped into the system, more bonds are broken and the system loses its connectedness [49]. The order parameter for the transition between an unconnected and a connected system is the fraction of sites in the infinite cluster P_∞.

Treating the static impurities as an average effect results in $P_\infty(z) = \langle p(\mathbf{r}) \rangle = 1 - z$, where z is the zinc concentration [55]. This fraction gives a constraint on the coherent spin, such that $\mathbf{\Omega}_I^2 = P_\infty$ instead of $\mathbf{\Omega}_I^2 = 1$ for the undoped system. The average effect on two sites, $\langle p_I p_J \rangle = K(\mathbf{r})$, where K is the bond dilution factor, which depends on the symmetry of the system's structure. Averaging also over the positions gives $\langle K(\mathbf{r}) \rangle = K(z) = 1 - 3z$, the average bond dilution factor as a function of the zinc concentration z for small z, which is the factor showing up in the Hamiltonians (3.9)-(3.11).

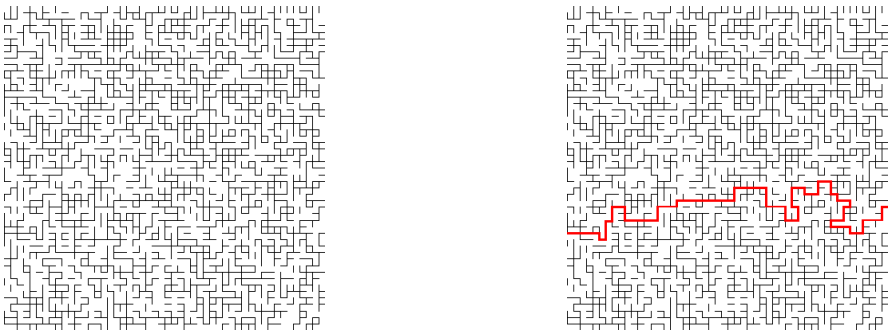

(a) (b)

Figure 3.2: (a) Abstract picture of the breaking of interaction bonds due to the dilution with zinc atoms in the copper lattice [54]. (b) Example of a connection from one side of the system to the other over the interaction bonds between the copper sites [56].

3.1.1 Wess-Zumino term

In going to the continuum limit in the expanded Heisenberg model, an additional term arises, such that the total partition function for the generalized nonlinear σ model contains not only the different terms of the Hamiltonian described above, but also a topological term that emerges as a Berry phase from the geometry of the coherent spin space that $\mathbf{\Omega}$ lives in [7]. This topological term is found by making a path integral expansion of the partition function

$$\mathcal{Z} = \operatorname{Tr} e^{-\beta H[\mathbf{S}]} = \int \mathrm{D}\mathbf{\Omega}\, \langle \mathbf{\Omega}| e^{-\beta H[\mathbf{S}]} |\mathbf{\Omega}\rangle = \int \prod \mathrm{D}\mathbf{\Omega}_i\, \langle \mathbf{\Omega}_i| e^{-\Delta\tau H[\mathbf{S}]} |\mathbf{\Omega}_{i+1}\rangle\,, \tag{3.12}$$

with $\Delta\tau = \beta/M$ an infinitesimal interval and M a large number. Expanding the exponent to first order in $\Delta\tau$ one finds that

$$\begin{aligned} \langle \mathbf{\Omega}_i| e^{-\Delta\tau H[\mathbf{S}]} |\mathbf{\Omega}_{i+1}\rangle &\approx \langle \mathbf{\Omega}_i| 1 - \Delta\tau H[\mathbf{S}] |\mathbf{\Omega}_{i+1}\rangle \approx \langle \mathbf{\Omega}_i| \Big(1 - \Delta\tau H[\mathbf{S}]\Big) \Big(|\mathbf{\Omega}_i\rangle + \Delta\tau \partial_\tau |\mathbf{\Omega}_i\rangle \Big) \\ &\approx 1 + \Delta\tau \langle \mathbf{\Omega}_i| \partial_\tau |\mathbf{\Omega}_i\rangle - \Delta\tau \langle \mathbf{\Omega}_i| H[\mathbf{S}] |\mathbf{\Omega}_i\rangle \\ &\approx e^{\Delta\tau(\langle \mathbf{\Omega}_i| \partial_\tau |\mathbf{\Omega}_i\rangle - H[S\mathbf{\Omega}_i])}. \end{aligned} \tag{3.13}$$

The partition function then becomes

$$\mathcal{Z} = \int \mathrm{D}\mathbf{\Omega} e^{\int_0^\beta \langle \mathbf{\Omega}| \partial_\tau |\mathbf{\Omega}\rangle - H[S\mathbf{\Omega}]\, \mathrm{d}\tau}, \tag{3.14}$$

where the integral over $\langle \mathbf{\Omega}| \partial_\tau |\mathbf{\Omega}\rangle$ corresponds to the Berry phase. Due to the periodic boundary conditions in τ and the requirement that $\mathbf{\Omega}^2 = 1$, this integral is a line integral over a closed curve on the parameter sphere, described by $\mathbf{\Omega}(\tau)$ as depicted in figure 3.3. The integral can therefore

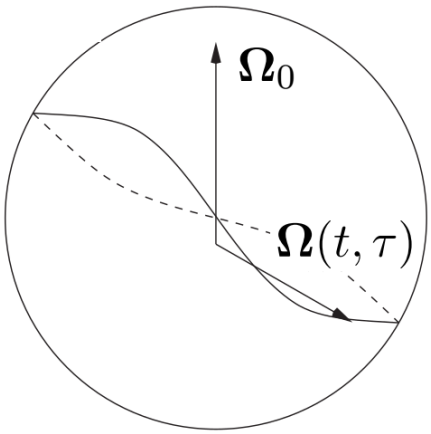

Figure 3.3: The trajectory travelled by the transformation of $\mathbf{\Omega}$ [57]. It splits the spin sphere into two surfaces.

be rewritten as

$$\begin{aligned}\int \langle \mathbf{\Omega}|\partial_\tau|\mathbf{\Omega}\rangle \,\mathrm{d}\tau &= -i \oint i \,\langle \mathbf{\Omega}|\nabla_{\mathbf{\Omega}}|\mathbf{\Omega}\rangle \cdot \mathrm{d}\mathbf{\Omega} \\ &= -\frac{i}{2}\int_{S^2} i\boldsymbol{\nabla} \times \langle \mathbf{\Omega}|\nabla_{\mathbf{\Omega}}|\mathbf{\Omega}\rangle \cdot \mathrm{d}^2\mathbf{\Omega} \\ &= -\frac{i}{2}\int_{S^2} \mathbf{B}\cdot \mathrm{d}^2\mathbf{\Omega}\,,\end{aligned} \tag{3.15}$$

where $\mathbf{B}$ is the Berry curvature, corresponding to the "flux" of a spin monopole in the center of the coherent spin sphere. In the transition from the line integral to the surface integral, Stokes' theorem was used. Note that there are two possible surfaces, the upper and the lower cap, and both should have the same surface integral, effectively giving half the integral over the whole sphere. The total flux over the sphere is quantized by an integer n and points along the surface normal, which is parallel to $\mathbf{\Omega}$. The integral for $n = 1$ then becomes

$$\int \langle \mathbf{\Omega}|\partial_\tau|\mathbf{\Omega}\rangle \,\mathrm{d}\tau = -\frac{i}{2}\int_{S^2} \mathbf{\Omega}\cdot \mathrm{d}^2\mathbf{\Omega}\,. \tag{3.16}$$

This simple surface integral can be evaluated by parametrizing the curve that $\mathbf{\Omega}$ describes with parameters $\tau \in [0, \beta]$ and $t \in [0, 1]$. The surface is then given by the normal vector times $\mathbf{\Omega}(t, \tau)$, so that the integral becomes

$$\int \langle \mathbf{\Omega}|\partial_\tau|\mathbf{\Omega}\rangle \,\mathrm{d}\tau = -\frac{i}{2}\int_0^\beta \int_0^1 \mathbf{\Omega}\cdot(\partial_\tau\mathbf{\Omega}\times\partial_t\mathbf{\Omega})\,\mathrm{d}t\,\mathrm{d}\tau \tag{3.17}$$

and, as a result, the partition function is

$$\mathcal{Z} = \int \mathrm{D}\mathbf{\Omega}\, e^{\mathcal{S}_{WZ} - \int_0^\beta H[S\mathbf{\Omega}]\mathrm{d}\tau}. \tag{3.18}$$

where the first term is given by the so-called Wess-Zumino action

$$\mathcal{S}_{WZ} = -iS\int_0^1 \int_0^\beta \mathbf{\Omega}\cdot(\partial_\tau\mathbf{\Omega}\times\partial_t\mathbf{\Omega})\,\mathrm{d}\tau\,\mathrm{d}t\,. \tag{3.19}$$

Applying again the spin decomposition from equation (3.6), the scalar triple product of the spin becomes to first order in a

$$\mathbf{\Omega}_I\cdot(\partial_\tau\mathbf{\Omega}_I\times\partial_t\mathbf{\Omega}_I) = \mathbf{n}_I\cdot\left[(-1)^I(\partial_\tau\mathbf{n}_I\times\partial_t\mathbf{n}_I) + a(\partial_\tau\mathbf{n}_I\times\partial_t\mathbf{l}_I) + a(\partial_\tau\mathbf{l}_I\times\partial_t\mathbf{n}_I)\right]. \tag{3.20}$$

The first term vanishes in the sum over the whole lattice for smooth configurations of $\mathbf{n}$, due to the terms with $(-1)^I$. The second and third term can be written as

$$\mathbf{n}_I\cdot(\partial_\tau\mathbf{n}_I\times\partial_t\mathbf{l}_I) = \partial_t\left[\mathbf{n}_I\cdot(\partial_\tau\mathbf{n}_I\times\mathbf{l}_I)\right] - \partial_t\mathbf{n}_I\cdot(\partial_\tau\mathbf{n}_I\times\mathbf{l}_I) = \partial_t\left[\mathbf{n}_I\cdot(\partial_\tau\mathbf{n}_I\times\mathbf{l}_I)\right] \tag{3.21}$$

$$\mathbf{n}_I\cdot(\partial_\tau\mathbf{l}_I\times\partial_t\mathbf{n}_I) = \partial_\tau\left[\mathbf{n}_I\cdot(\mathbf{l}_I\times\partial_t\mathbf{n}_I)\right] - \partial_\tau\mathbf{n}_I\cdot(\mathbf{l}_I\times\partial_t\mathbf{n}_I) = \partial_\tau\left[\mathbf{n}_I\cdot(\mathbf{l}_I\times\partial_t\mathbf{n}_I)\right], \tag{3.22}$$

where the extra terms on the right-hand side vanish, because the vectors $\mathbf{l}_I$, $\partial_t \mathbf{n}_I$ and $\partial_\tau \mathbf{n}_I$ are coplanar. It is assumed that there is no contribution from second derivatives in $\mathbf{n}_I$. The integral over τ of equation (3.22) becomes zero due to the periodic boundary conditions in τ, while the t-integral over the right-hand side of equation (3.21) results in

$$\int_0^1 \partial_t \left[\mathbf{n}_I \cdot (\partial_\tau \mathbf{n}_I \times \mathbf{l}_I)\right] \mathrm{d}t = \mathbf{n}_I \cdot (\partial_\tau \mathbf{n}_I \times \mathbf{l}_I), \tag{3.23}$$

because $\partial_\tau \mathbf{n}_I(t=0) = 0$. The integral of the term from equation (3.20) is therefore reduced to

$$\int_0^1 \int_0^\beta \mathbf{\Omega}_I \cdot (\partial_\tau \mathbf{\Omega}_I \times \partial_t \mathbf{\Omega}_I)\, \mathrm{d}\tau\, \mathrm{d}t = \int_0^\beta \mathbf{n}_I \cdot (\partial_\tau \mathbf{n}_I \times \mathbf{l}_I)\, \mathrm{d}\tau\,. \tag{3.24}$$

Substituting this back into the Wess-Zumino action of equation (3.19) leads, in the continuum limit and including again percolation, to

$$\mathcal{S}_{WZ} = \frac{-iSP_\infty}{a} \int_0^\beta \mathrm{d}\tau \int \mathrm{d}^2\mathbf{r}\, \mathbf{l} \cdot (\mathbf{n} \times \partial_\tau \mathbf{n})\,, \tag{3.25}$$

where $P_\infty = \langle p(\mathbf{r}) \rangle$ is again the fraction of sites in the infinite cluster [49]. It enters here instead of $K(z)$ as for the other terms, because the Wess-Zumino action goes as $\mathbf{\Omega}_I^3 \propto p_I^3 = p_I$, where $p_I = 1$ at copper sites and $p_I = 0$ at zinc sites.

3.1.2 Generalized nonlinear σ model and the Néel temperature $T_N(z)$

The full action for the generalized nonlinear σ model is the sum of the Heisenberg, DM interaction, XY interaction and the Wess-Zumino actions [49]. In terms of the staggered and uniform spin fields, it is given by

$$\begin{aligned}\mathcal{S}_{gnl\sigma m} = \iint \Bigg[& -i\frac{SP_\infty}{a}\, \mathbf{l} \cdot (\mathbf{n} \times \partial_\tau \mathbf{n}) + \frac{JS^2K}{2} \left((\nabla \mathbf{n})^2 + 8\mathbf{l}^2\right) \\ & + \frac{4S^2K}{a}\, \mathbf{d}_+ \cdot (\mathbf{n} \times \mathbf{l}) + \frac{2S^2K}{a^2} (\Gamma_1 - \Gamma_3) n_z^2 \Bigg] \mathrm{d}^2\mathbf{r}\, \mathrm{d}\tau\,.\end{aligned} \tag{3.26}$$

The first step now is to integrate out the uniform field $\mathbf{l}(\mathbf{r})$ in the partition function using the typical Gaussian integral for a vector, which results in

$$\begin{aligned}\int \mathrm{D}\mathbf{l}\, e^{\iint 4S^2JK|\mathbf{l}|^2 + \mathbf{l}\cdot\left(-i\frac{SP_\infty}{a}\mathbf{n}\times\partial_\tau\mathbf{n} - \frac{4S^2K}{a}\mathbf{n}\times\mathbf{d}_+\right)\mathrm{d}^2\mathbf{r}\mathrm{d}\tau} &\propto e^{-\frac{1}{16JS^2K}\iint\left(-i\frac{SP_\infty}{a}\mathbf{n}\times\partial_\tau\mathbf{n} - \frac{4S^2K}{a}\mathbf{n}\times\mathbf{d}_+\right)^2 \mathrm{d}^2\mathbf{r}\mathrm{d}\tau} \\ &= e^{\iint \frac{P_\infty}{16JKa}(\partial_\tau\mathbf{n})^2 - \frac{S^2K}{Ja^2}\left(\mathbf{d}_+^2 - (\mathbf{n}\cdot\mathbf{d}_+)^2\right) - \frac{iSP_\infty}{8Ja^2}(\partial_\tau\mathbf{n}\cdot\mathbf{d}_+)\,\mathrm{d}^2\mathbf{r}\mathrm{d}\tau},\end{aligned} \tag{3.27}$$

where it was used that $\mathbf{n}^2 = 1$ and $\mathbf{n} \cdot \partial_\tau \mathbf{n} = 0$. The integral of the last term $\partial_\tau \mathbf{n} \cdot \mathbf{d}_+$ vanishes due to the periodicity of $\mathbf{n}(\tau)$ in τ. In the middle term, the $\mathbf{d}_+^2$-part only shifts the action by a constant, so that it can be neglected and the resulting total action is

$$\mathcal{S}_{gnl\sigma m} = \frac{1}{2gc} \int \mathrm{d}\tau \int \mathrm{d}^2\mathbf{r} \left[\frac{P_\infty}{K} (\partial_\tau \mathbf{n})^2 + Kc^2 (\nabla \mathbf{n})^2 + K\mathbf{D}_+^2 n_a^2 + K\Gamma_c n_c^2 \right], \tag{3.28}$$

where $g = 2\sqrt{2}a/S$ is the bare coupling constant, $c = 2\sqrt{2}SJa$ is the spin-wave velocity, $\mathbf{D}_+ = 4S\mathbf{d}_+$, n_a and n_c are the components of the staggered spin field in the **a**-orthorhombic and **c** direction, respectively, and $\Gamma_c = 32JS^2(\Gamma_1 - \Gamma_3)$. In a more conventional notation, this can be redefined as

$$\mathcal{S}_{gnl\sigma m} = \frac{1}{2gcK/P_\infty} \int d\tau \int d^2\mathbf{r} \left[(\partial_\tau \mathbf{n})^2 + Z \left\{ c^2 (\nabla \mathbf{n})^2 + m_a^2 n_a^2 + m_c^2 n_c^2 \right\} \right], \tag{3.29}$$

where $Z = K^2/P_\infty$, $m_a = D_+$ and $m_c^2 = \Gamma_c$. From this action one can see that the favoured orientation of the antiferromagnetic spin $\mathbf{n}$ is along the **b**-orthorhombic direction, as the **a**- and **c**-directions give an energy penalty due to the mass terms [58]. So it makes sense to split the staggered field $\mathbf{n}$ into a parallel and a perpendicular component compared to the $\mathbf{b}_{ortho}$-direction, so that $\mathbf{n} = (n_a, n_b = \sigma_0, n_c) = (\sigma_0, \mathbf{n}_\perp)$, where σ_0 is a constant [49]. With a Lagrange multiplier to ensure the constraint that $\mathbf{n}^2 = P_\infty$ from percolation, the partition function becomes

$$\begin{aligned} \mathcal{Z} &= \int \mathrm{D}\sigma_0 \mathrm{D}\mathbf{n}_\perp \delta \left(\mathbf{n}^2 - P_\infty \right) e^{-S[\sigma_0, \mathbf{n}_\perp]} \\ &= \int \mathrm{D}\sigma_0 \mathrm{D}\mathbf{n}_\perp \mathrm{D}\lambda \, e^{\frac{1}{2gcK/P_\infty} \mathrm{Tr}\left[n_\perp \left(\omega_n^2 + Zc^2\mathbf{k}^2 + Zm_a^2 + Zm_c^2 + i\lambda \right) n_\perp + i\lambda\sigma_0^2 - i\lambda P_\infty \right]}, \end{aligned} \tag{3.30}$$

where $\mathrm{Tr} = \frac{1}{\beta} \sum_{n=-\infty}^{\infty} \int \frac{\mathrm{d}^2\mathbf{k}}{(2\pi)^2}$, i.e. the Matsubara sum and the momentum space integral. After one integrates out the transverse field component $\mathbf{n}_\perp$, one obtains, up to a constant,

$$\mathcal{Z} = \int \mathrm{D}\sigma_0 \mathrm{D}\lambda \, e^{\frac{1}{2gcK/P_\infty} \mathrm{Tr}\left[i\lambda\sigma_0^2 - i\lambda P_\infty \right] - \frac{1}{2} \mathrm{Tr} \ln \left[\omega_n^2 + \zeta^2 \right]}, \tag{3.31}$$

where $\zeta^2 = i\lambda + Z(c^2\mathbf{k}^2 + m_a^2 + m_c^2)$. Varying the action of this partition function with respect to σ_0 and λ gives the equations of state for the system

$$\lambda\sigma_0 = 0, \tag{3.32}$$

$$\frac{P_\infty - \sigma_0^2}{gcK/P_\infty} = \mathrm{Tr} \, \frac{1}{\omega_n^2 + \zeta^2}, \tag{3.33}$$

where the Lagrange multiplier λ is related to the correlation length by $\lambda \sim \xi^{-2}$ [58]. There are three different regimes that satisfy the first of the above equations, namely $\langle \sigma_0 \rangle = 0$, $\lambda = 0$ or both $\sigma_0 = \lambda = 0$. In the first case where $\langle \sigma_0 \rangle = 0$, the main spin component averages to zero, so the

system is in the paramagnetic phase, $T > T_N$, and the correlation length is finite, $\lambda = 1/\xi^2 > 0$. In the second regime with $\lambda = 0$, the correlation length goes to infinity and the system is in the antiferromagnetic phase with $T < T_N$. At the point where both the average spin and the inverse correlation length reach zero, the phase transition occurs.

At this critical point $T = T_N$, equation (3.33) becomes [49]

$$\frac{P_\infty^2}{gcK} = \mathrm{Tr}\,\frac{1}{\omega_n^2 + \zeta^2}. \tag{3.34}$$

The first step in working with this equation is performing the Matsubara sum

$$\begin{aligned}\frac{1}{\beta}\sum_{n=-\infty}^{\infty}\frac{1}{(2\pi n/\beta)^2+\zeta^2} &= \frac{\beta}{(2\pi)^2}\sum_{n=-\infty}^{\infty}\frac{1}{n^2+(\beta\zeta/2\pi)^2}\\ &= \frac{\beta}{(2\pi)^2}\frac{\pi\coth(\pi\beta\zeta/2\pi)}{\beta\zeta/2\pi}\\ &= \frac{1}{2\zeta}\coth\frac{\beta\zeta}{2}.\end{aligned} \tag{3.35}$$

Then equation (3.34) becomes

$$\begin{aligned}\frac{P_\infty^2}{gcK} &= \int\frac{\mathrm{d}^2\mathbf{k}}{(2\pi)^2}\frac{1}{2c\sqrt{Z(\mathbf{k}^2+(m_a^2+m_c^2)/c^2)}}\coth\frac{c\beta\sqrt{Z(\mathbf{k}^2+(m_a^2+m_c^2)/c^2)}}{2}\\ &= \frac{1}{2\pi Zc^2\beta}\int_{\beta\sqrt{Z(m_a^2+m_c^2)}/2}^{\beta c\Lambda/2}\coth y\,\mathrm{d}y\\ &= \frac{1}{2\pi\beta c^2 Z}\left[\ln\sinh\frac{\beta c\Lambda}{2}-\ln\sinh\frac{\beta\sqrt{Z(m_a^2+m_c^2)}}{2}\right],\end{aligned} \tag{3.36}$$

with a change of variables $y = \frac{c\beta\sqrt{Z}}{2}\sqrt{\mathbf{k}^2+(m_a^2+m_c^2)/c^2}$ and $\Lambda = \sqrt{2\pi}/a$ the Fermi cut-off. This can be rearranged into

$$\frac{2\pi\beta cKP_\infty}{g} - \ln\sinh\frac{2\pi\beta c}{g_c} + \ln\sinh\frac{\beta\sqrt{Z(m_a^2+m_c^2)}}{2} = 0, \tag{3.37}$$

where $g_c = 4\pi/\Lambda$ is a critical coupling constant. However, the cut-off Λ diverges in the continuum limit where the lattice spacing goes to zero. Using that $\lim_{x\to\infty}\ln\sinh x = \ln(e^x/2) = x - \ln 2$, and defining the so-called spin stiffness as

$$\rho_s = c\left(\frac{1}{2g} - \frac{1}{2g_cKP_\infty}\right), \tag{3.38}$$

the equation describing the Néel temperature $k_B T_N = 1/\beta_N$ is given by

$$4\pi\beta_N P_\infty K\rho_s + \ln\left[2\sinh\frac{\beta_N\sqrt{Z(m_a^2+m_c^2)}}{2}\right] = 0. \tag{3.39}$$

In the undoped system, the Néel temperature would be governed by

$$4\pi\beta_N\rho_s + \ln\left[2\sinh\frac{\beta_N\sqrt{m_a^2+m_c^2}}{2}\right] = 0. \tag{3.40}$$

This shows that the dilution from the zinc doping changes the system by a rescaling of the spin stiffness and the anisotropy mass. The spin stiffness is an indication of the change in the ground state energy of a spin system caused by a slow in-plane twist of the spins [59]. It is often used as an indicator of quantum phase transitions. The anisotropy masses correspond to DM and XY gaps, that get renormalized by a factor of $\sqrt{Z}$. The DM gap is the in-plane gap, while the XY gap is the out-of-plane gap. Both result in an easier destruction of the Néel ground state by thermal fluctuations, decreasing the Néel temperature with increasing zinc concentration, see figure 3.4.

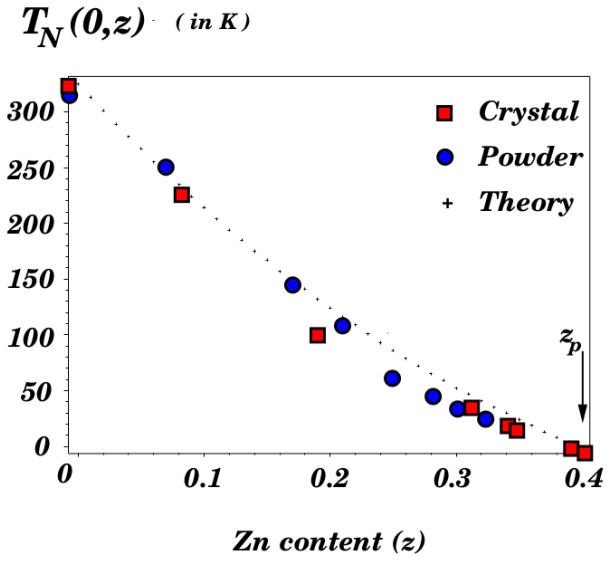

Figure 3.4: The decrease in the Néel temperature as a function of the zinc concentration with data from experiments and theory, taken from Ref. [55].

3.2 Hole doping

As mentioned in section 2.2, the charge carriers responsible for superconductivity in the cuprates are the holes that are added to the copper-oxygen plane by doping the spacer layers with strontium. These additional holes are the itinerant holes, which hop between the oxygen ions, while the initial holes from the undoped material are localized on the copper atoms. Both types of holes can be described by the Spin-Fermion-Hubbard (SFH) model proposed by Marino *et al.* [60], which contains besides the hopping energy also on-site Coulomb repulsions, antiferromagnetic superexchange interactions between the copper atoms' holes and Kondo magnetic interactions between the localized and the itinerant holes. The goal of this section is to describe the critical temperature $T_c(x)$ that forms the dome of the superconducting phase in the phase diagram of $La_{2-x}Sr_xCuO_4$ as a function of the doping concentration x. For this, the SFH model will be used, following Marino *et al.* [60].

The underlying structure for the model is again the copper-oxygen plane, but now the focus is on the oxygen sites instead of the copper sites. The oxygen ions couple in two distinct ways with the copper ions, namely with either their p_x or their p_y orbital overlapping with the copper d-orbital. This leads to two different sublattices for the oxygen atoms. The lattice from the point of view of the oxygen sites can be seen in figure 3.5. The lattice vectors are

$$\mathbf{d}_1 = \frac{1}{2}\left(\mathbf{X} - \mathbf{Y}\right), \tag{3.41}$$

$$\mathbf{d}_2 = \frac{1}{2}\left(\mathbf{X} + \mathbf{Y}\right), \tag{3.42}$$

$$\mathbf{d}_3 = \frac{1}{2}\left(-\mathbf{X} + \mathbf{Y}\right), \tag{3.43}$$

$$\mathbf{d}_4 = \frac{1}{2}\left(-\mathbf{X} - \mathbf{Y}\right), \tag{3.44}$$

where $\mathbf{X} = a\hat{x}$ and $\mathbf{Y} = a\hat{y}$ are the primitive vectors of the copper lattice (a is again the lattice spacing between the copper atoms).

The Spin-Fermion-Hubbard Hamiltonian for the holes in the copper-oxygen plane is given by

$$H_{SFH} = H_0 + H_U + H_{AF} + H_K \tag{3.45}$$

where H_0 is the kinetic hopping term, H_U is the on-site Coulomb repulsion for the itinerant holes in the different sublattices, H_{AF} is the antiferromagnetic interaction for the localized holes, and H_K is the magnetic interaction with the spins of the itinerant holes. These individual terms are

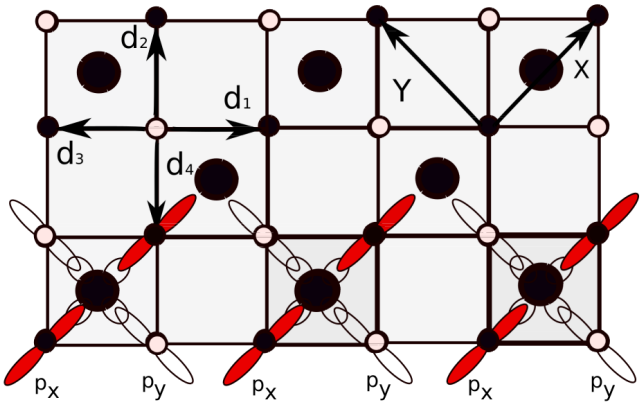

Figure 3.5: Square lattice for the copper-oxygen plane [60]. The small black and the small white dots are the two different types of oxygen ions, with only their p_x or p_y shells contributing, respectively, while the large black dots are the copper atoms. The vectors $\mathbf{X}$ and $\mathbf{Y}$ are the primitive vectors for the copper lattice, while the $\mathbf{d}_i$ form the oxygen lattice.

given by

$$H_0 = -t_p \sum_{\sigma,\mathbf{R},\mathbf{d}_i} \left[\psi^\dagger_{A\sigma}(\mathbf{R})\psi_{B\sigma}(\mathbf{R}+\mathbf{d}_i) + \psi^\dagger_{B\sigma}(\mathbf{R}+\mathbf{d}_i)\psi_{A\sigma}(\mathbf{R})\right], \tag{3.46}$$

$$H_U = U_p \sum_{\mathbf{R}} n^A_\uparrow n^A_\downarrow + U_p \sum_{\mathbf{R},\mathbf{d}_i} n^B_\uparrow n^B_\downarrow, \tag{3.47}$$

$$H_{AF} = J_{AF} \sum_{\langle I,\, J\rangle} \mathbf{S}_I \cdot \mathbf{S}_J, \tag{3.48}$$

$$H_K = J_K \sum_{I,\mathbf{R},\mathbf{d}_i} \mathbf{S}_I \cdot \left[\mathbf{S}_A(\mathbf{R}) + \mathbf{S}_B(\mathbf{R}+\mathbf{d}_i)\right], \tag{3.49}$$

with the sums taken over the nearest neighbours, $\mathbf{R}$ the position on the A-sublattice of the oxygen atoms, $\mathbf{R}+\mathbf{d}_i$ the position of the surrounding oxygen atoms on the B-sublattice, and I, J the positions of the copper atoms. Here, t_p is the parameter for the hole hopping between oxygen sites on the different sublattices A and B, U_p is the onsite interaction, J_{AF} the antiferromagnetic coupling strength between holes on the copper sites and J_K the Kondo coupling parameter for the interaction between the holes on the copper and the holes on the oxygen sites. The coupling

parameters are related to the three-band model as described in section 2.2.2 with [61]

$$J_{AF} = \frac{4t_{pd}^4}{(U_{pd}+\Delta_E)^2}\left(\frac{1}{U_d}+\frac{2}{2\Delta_E+U_p}\right), \tag{3.50}$$

$$J_K = t_{pd}^2\left(\frac{1}{\Delta_E}+\frac{1}{U_d-\Delta_E}\right), \tag{3.51}$$

where $\Delta_E = \epsilon_p - \epsilon_d$ is the energy difference between the oxygen and the copper orbits, t_d is the copper hopping parameter and the other parameters as explained before.

3.2.1 Effective Hamiltonian

The first step in dealing with the Hamiltonian H_{SFH} is to trace out the localized spins of the copper atoms in a similar way as in section 3.1 in the partition function

$$\mathcal{Z} = \mathrm{Tr}_\psi \,\mathrm{Tr}_{\mathbf{S}_I}\, e^{-\beta H_{SFH}[\mathbf{S}_I,\psi]} = \mathrm{Tr}_\psi \left(e^{-\beta(H_0[\psi]+H_U[\psi])}\,\mathrm{Tr}_{\mathbf{S}_I}\, e^{-\beta(H_{AF}[\mathbf{S}_I]+H_K[\mathbf{S}_I,\psi])}\right). \tag{3.52}$$

The trace over the localized spins $\mathbf{S}_I$ can be performed by transitioning to the spin coherent states $\mathbf{\Omega}_I \equiv \mathbf{S}_I/S$, leading to the path integral

$$\mathrm{Tr}_{\mathbf{S}_I}\, e^{-\beta\left(H_{AF}[\mathbf{S}_I]+H_K[\mathbf{S}_I,\psi]\right)} = \int \mathrm{D}\mathbf{\Omega}\ \langle\mathbf{\Omega}|e^{-\beta H[\mathbf{S}_I]}|\mathbf{\Omega}\rangle \approx \int \mathrm{D}\mathbf{\Omega}\, e^{\int_0^\beta \langle\mathbf{\Omega}(\tau)|\partial_\tau|\mathbf{\Omega}(\tau)\rangle - H[S\mathbf{\Omega}]\,\mathrm{d}\tau}, \tag{3.53}$$

where $H[S\mathbf{\Omega}] = S^2 J_{AF}\sum_{\langle I,\,J\rangle}\mathbf{\Omega}_I\cdot\mathbf{\Omega}_J + SJ_K\sum_{\langle I,\,J\rangle}\mathbf{\Omega}_I\cdot(\mathbf{S}_A+\mathbf{S}_B)$. The spin state may again be split into an antiferromagnetic and a fluctuating component, but now according to

$$\mathbf{\Omega}_I \approx (-1)^I\mathbf{n}_I + a^2\mathbf{l}_I \tag{3.54}$$

where $\mathbf{n}_I$ is the staggered unit spin and $\mathbf{l}_I$ is the perpendicular fluctuation, obeying as before the relations $|\mathbf{n}|^2 = 1$ and $\mathbf{n}\cdot\mathbf{l} = 0$. The nearest neighbour's spin at site $J = I+1$ is approximated by an expansion around the spin of site I

$$\mathbf{\Omega}_J \approx (-1)^{I+1}\mathbf{n}_I + a\nabla\mathbf{n}_I + a^2\mathbf{l}_I. \tag{3.55}$$

With this, following the same steps as in section 3.1.1 leads to the term from equation (3.25) without the percolation factor for the Berry phase term in equation (3.53). In the Hamiltonian term $H[S\mathbf{\Omega}]$ one has

$$\mathbf{\Omega}_I\cdot\mathbf{\Omega}_J \propto \frac{1}{2}\left(\mathbf{\Omega}_I+\mathbf{\Omega}_J\right)^2 \approx a^2(\nabla\mathbf{n}_I)^2 + 4a^3\nabla\mathbf{n}_I\cdot\mathbf{l}_I + 4a^4|\mathbf{l}_I|^2, \tag{3.56}$$

where some constant factors were neglected, and

$$\mathbf{\Omega}_I\cdot(\mathbf{S}_A+\mathbf{S}_B) \approx \left[(-1)^I\mathbf{n}_I + a^2\mathbf{l}_I\right]\cdot(\mathbf{S}_A+\mathbf{S}_B). \tag{3.57}$$

Because of the symmetry of the lattice and the continuity of $\mathbf{n}$, the middle term of equation (3.56) and the first term of equation (3.57) vanish, so that in the continuum limit

$$H[\mathbf{n},\mathbf{l}] = \frac{S^2 J_{AF}}{2}\int \left[(\nabla \mathbf{n}(\mathbf{r}))^2 + 4a^2|\mathbf{l}|^2\right] \mathrm{d}^2\mathbf{r} + SJ_K \int \mathbf{l}\cdot(\mathbf{S}_A+\mathbf{S}_B)\,\mathrm{d}^2\mathbf{r}\,. \tag{3.58}$$

As a result, the full trace over the spins in the partition function can be written as

$$\int \mathrm{D}\mathbf{\Omega}\, e^{\int_0^\beta \langle \mathbf{\Omega}(\tau)|\partial_\tau|\mathbf{\Omega}(\tau)\rangle - H[S\mathbf{\Omega}]\,\mathrm{d}\tau} = \int \mathrm{D}\mathbf{n}\mathrm{D}\mathbf{l}\,\delta(\mathbf{n}^2-1)\, e^{\iint\left[i\mathbf{l}\cdot(\mathbf{n}\times\partial_\tau\mathbf{n}) - \frac{S^2J_{AF}}{2}(\nabla\mathbf{n})^2 - \frac{S^2J_{AF}}{2}4a^2|\mathbf{l}|^2 - SJ_K\mathbf{l}\cdot(\mathbf{S}_A+\mathbf{S}_B)\right]\mathrm{d}^2\mathbf{r}\mathrm{d}\tau}, \tag{3.59}$$

where the integral over the fluctuating field $\mathbf{l}$ is a simple Gaussian integral with a linear term, and gives

$$\begin{aligned}\int \mathrm{D}\mathbf{l}\, e^{-\iint\left[\frac{4S^2J_{AF}a^2}{2}|\mathbf{l}|^2 + \mathbf{l}\cdot(SJ_K(\mathbf{S}_A+\mathbf{S}_B) - i\mathbf{n}\times\partial_\tau\mathbf{n})\right]\mathrm{d}^2\mathbf{r}\mathrm{d}\tau} &\propto e^{\iint \frac{1}{2}[SJ_K(\mathbf{S}_A+\mathbf{S}_B) - i\mathbf{n}\times\partial_\tau\mathbf{n}]^2 \frac{1}{4S^2J_{AF}a^2}\mathrm{d}^2\mathbf{r}\mathrm{d}\tau} \\ &= e^{\iint \frac{J_K^2}{8J_{AF}a^2}(\mathbf{S}_A+\mathbf{S}_B)^2\mathrm{d}^2\mathbf{r}\mathrm{d}\tau} e^{-\iint \frac{1}{8S^2J_{AF}a^2}(\partial_\tau\mathbf{n})^2\mathrm{d}^2\mathbf{r}\mathrm{d}\tau},\end{aligned} \tag{3.60}$$

where it was used that the cross term between the oxygen spins and the uniform field $\mathbf{n}$ vanishes. The remaining integral is then given by

$$\int \mathrm{D}\mathbf{n}\,\delta(\mathbf{n}^2-1) e^{-\frac{\rho}{2}\iint\left[(\nabla\mathbf{n})^2 + \frac{1}{c^2}(\partial_\tau\mathbf{n})^2\right]\mathrm{d}^2\mathbf{r}\mathrm{d}\tau} e^{\iint \frac{J_K^2}{8J_{AF}a^2}(\mathbf{S}_A+\mathbf{S}_B)^2\mathrm{d}^2\mathbf{r}\mathrm{d}\tau} = \mathcal{Z}_{nl\sigma m} e^{\int_0^\beta \sum_{\mathbf{R},\mathbf{d}_i}\frac{J_K^2}{8J_{AF}}(\mathbf{S}_A+\mathbf{S}_B)^2\mathrm{d}\tau}, \tag{3.61}$$

with $\rho = S^2 J_{AF}$ the spin stiffness and $c = 2S^2 J_{AF} a$ the spin-wave velocity. Finally, the total partition function becomes

$$\mathcal{Z} = \mathcal{Z}_{nl\sigma m}\,\mathrm{Tr}_\psi\, e^{-\beta\left(H_0 + H_U - \sum_{\mathbf{R},\mathbf{d}_i}\frac{J_K^2}{8J_{AF}}(\mathbf{S}_A+\mathbf{S}_B)^2\right)} \tag{3.62}$$

and one is left with an effective Hamiltonian for only the itinerant holes. The spin operators in this effective Hamiltonian can be expressed in terms of the hole creation and annihilation operators for the two sublattices according to

$$\mathbf{S}_A(\mathbf{R}) = \frac{1}{2}\psi^\dagger_{A,\alpha}(\mathbf{R})\sigma_{\alpha\beta}\psi_{A\beta}(\mathbf{R}), \tag{3.63}$$

$$\mathbf{S}_B(\mathbf{R}+\mathbf{d}_i) = \frac{1}{2}\psi^\dagger_{B,\alpha}(\mathbf{R}+\mathbf{d}_i)\sigma_{\alpha\beta}\psi_{B\beta}(\mathbf{R}+\mathbf{d}_i), \tag{3.64}$$

where $\sigma_{\alpha\beta}$ are the spin Pauli matrices.

Including a perturbation in the hopping term and the on-site repulsion, one finds for the effective Hamiltonian in terms of the hole creation and annihilation fields

$$\begin{aligned} H_{eff} = &- t_p \sum_{\mathbf{R},\mathbf{d}_i,\sigma} \left[\psi^\dagger_{A\sigma}(\mathbf{R})\psi_{B\sigma}(\mathbf{R}+\mathbf{d}_i) + \psi^\dagger_{B\sigma}(\mathbf{R}+\mathbf{d}_i)\psi_{A\sigma}(\mathbf{R})\right] \\ &- g_S \sum_{\mathbf{R},\mathbf{d}_i} \left[\psi^\dagger_{A\uparrow}(\mathbf{R})\psi^\dagger_{B\downarrow}(\mathbf{R}+\mathbf{d}_i) + \psi^\dagger_{B\uparrow}(\mathbf{R}+\mathbf{d}_i)\psi^\dagger_{A\downarrow}(\mathbf{R})\right] \times \\ &\qquad \left[\psi_{B\downarrow}(\mathbf{R}+\mathbf{d}_i)\psi_{A\uparrow}(\mathbf{R}) + \psi_{A\downarrow}(\mathbf{R})\psi_{B\uparrow}(\mathbf{R}+\mathbf{d}_i)\right] \\ &- g_P \sum_{\mathbf{R},\mathbf{d}_i} \left[\psi^\dagger_{A\uparrow}(\mathbf{R})\psi_{B\uparrow}(\mathbf{R}+\mathbf{d}_i) + \psi^\dagger_{A\downarrow}(\mathbf{R})\psi_{B\downarrow}(\mathbf{R}+\mathbf{d}_i)\right] \times \\ &\qquad \left[\psi^\dagger_{B\uparrow}(\mathbf{R}+\mathbf{d}_i)\psi_{A\uparrow}(\mathbf{R}) + \psi^\dagger_{B\downarrow}(\mathbf{R}+\mathbf{d}_i)\psi_{A\downarrow}(\mathbf{R})\right], \end{aligned} \tag{3.65}$$

where $g_S = J_K^2/(8J_{AF})$ and $g_P = 2t_p^2/U_p$ are the superconducting and the pseudogap coupling parameters, respectively. The superconducting coupling corresponds to an attractive interaction between the holes.

The next step is to perform a Hubbard-Stratonovitch transformation to cancel the terms quadratic in the fermionic fields. This results in an effective Hamiltonian

$$\begin{aligned} H_{eff}[\Phi,\chi,\psi] = &- t_p \sum_{\mathbf{R},\mathbf{d}_i} \sum_{\sigma} \left[\psi^\dagger_{A\sigma}(\mathbf{R})\psi_{B\sigma}(\mathbf{R}+\mathbf{d}_i) + h.c.\right] \\ &- \sum_{\mathbf{R},\mathbf{d}_i} \left\{\Phi(\mathbf{d}_i)\left[\psi^\dagger_{A\uparrow}(\mathbf{R})\psi^\dagger_{B\downarrow}(\mathbf{R}+\mathbf{d}_i) + \psi^\dagger_{B\uparrow}(\mathbf{R}+\mathbf{d}_i)\psi^\dagger_{A\downarrow}(\mathbf{R})\right] + h.c.\right\} \\ &- \sum_{\mathbf{R},\mathbf{d}_i} \left\{\chi(\mathbf{d}_i)\left[\psi^\dagger_{A\uparrow}(\mathbf{R})\psi_{B\uparrow}(\mathbf{R}+\mathbf{d}_i) + \psi^\dagger_{A\downarrow}(\mathbf{R})\psi_{B\downarrow}(\mathbf{R}+\mathbf{d}_i)\right] + h.c.\right\} \\ &+ \frac{1}{g_S}\sum_{\mathbf{R},\mathbf{d}_i} \Phi^\dagger(\mathbf{R}+\mathbf{d}_i)\Phi(\mathbf{R}+\mathbf{d}_i) + \frac{1}{g_P}\sum_{\mathbf{R},\mathbf{d}_i} \chi^\dagger(\mathbf{R}+\mathbf{d}_i)\chi(\mathbf{R}+\mathbf{d}_i), \end{aligned} \tag{3.66}$$

where

$$\Phi^\dagger(\mathbf{R},\mathbf{d}_i) = g_S\left[\psi^\dagger_{A\uparrow}(\mathbf{R})\psi^\dagger_{B\downarrow}(\mathbf{R}+\mathbf{d}_i) + \psi^\dagger_{B\uparrow}(\mathbf{R}+\mathbf{d}_i)\psi^\dagger_{A\downarrow}(\mathbf{R})\right], \tag{3.67}$$

$$\chi^\dagger(\mathbf{R},\mathbf{d}_i) = g_P\left[\psi^\dagger_{A\uparrow}(\mathbf{R})\psi_{B\uparrow}(\mathbf{R}+\mathbf{d}_i) + \psi^\dagger_{A\downarrow}(\mathbf{R})\psi_{B\downarrow}(\mathbf{R}+\mathbf{d}_i)\right] \tag{3.68}$$

are the Cooper pair creation field and the exciton (electron-hole pair) creation field. These fields live on the links between the oxygen sites and are mostly translationally invariant, so that only the dependence on $\mathbf{d}_i$ matters. Similar to the BCS theory of section 2.1.2, the vacuum expectation values of these fields $\Delta = \langle\Phi\rangle$ and $M = \langle\chi\rangle$ give the order parameters for the superconducting

and the pseudogap phases, respectively. As in the before-mentioned section 2.1.2, the Fourier transformation of the effective Hamiltonian[1]

$$\begin{aligned} H_{eff}[\Phi,\chi,\psi](\mathbf{k}) = &- t\sum_{\mathbf{k},\sigma}\sum_{i=1}^{4}\left[e^{i\mathbf{k}\cdot\mathbf{d}_i}\psi^\dagger_{A\sigma}(\mathbf{k})\psi_{B\sigma}(\mathbf{k}) + h.c.\right] \\ &- \sum_{\mathbf{k}}\left\{\Phi(\mathbf{k})\left[\psi^\dagger_{A\uparrow}(-\mathbf{k})\psi^\dagger_{B\downarrow}(\mathbf{k}) + \psi^\dagger_{B\uparrow}(\mathbf{k})\psi^\dagger_{A\downarrow}(-\mathbf{k})\right] + h.c.\right\} \\ &- \sum_{\mathbf{k},\sigma}\left\{\chi(\mathbf{k})\left[\psi^\dagger_{A\sigma}(\mathbf{k})\psi_{B\sigma}(\mathbf{k})\right] + h.c.\right\} \\ &+ \frac{1}{g_S}\sum_{\mathbf{k}}\Phi^\dagger(\mathbf{k})\Phi(\mathbf{k}) + \frac{1}{g_P}\sum_{\mathbf{k}}\chi^\dagger(\mathbf{k})\chi(\mathbf{k}) \end{aligned} \tag{3.69}$$

can be expressed in terms of the Nambu fermion field

$$\Psi(\mathbf{k}) = \begin{pmatrix} \psi_{A,\uparrow}(\mathbf{k}) \\ \psi_{B,\uparrow}(\mathbf{k}) \\ \psi^\dagger_{A,\downarrow}(-\mathbf{k}) \\ \psi^\dagger_{B,\downarrow}(-\mathbf{k}) \end{pmatrix}. \tag{3.70}$$

Performing a mean-field approximation in the Hubbard-Stratonovitch fields, one can write the effective Hamiltonian in terms of the Nambu fields as

$$H_{eff}[\Delta, M, \Psi] = \frac{1}{g_S}\sum_{\mathbf{k}}|\Delta(\mathbf{k})|^2 + \frac{1}{g_P}\sum_{\mathbf{k}}|M(\mathbf{k})|^2 + \sum_{\mathbf{k}}\Psi^\dagger(\mathbf{k})\mathcal{H}(\mathbf{k})\Psi(\mathbf{k}), \tag{3.71}$$

where the matrix $\mathcal{H}$ is given by

$$\mathcal{H} = \begin{pmatrix} 0 & \epsilon - M & 0 & -\Delta \\ \epsilon - M^* & 0 & -\Delta & 0 \\ 0 & -\Delta^* & 0 & -\epsilon + M^* \\ -\Delta^* & 0 & -\epsilon + M & 0 \end{pmatrix}, \tag{3.72}$$

with $\epsilon = -t\sum_{k,i} e^{i\mathbf{k}\mathbf{d}_i}$. This matrix has the doubly degenerate energy eigenvalues

$$E(\mathbf{k}) = \pm\sqrt{\epsilon^2(\mathbf{k}) + |M(\mathbf{k})|^2 + |\Delta(\mathbf{k})|^2}. \tag{3.73}$$

At this point, it can be noted that the superconducting order parameter has a d-wave nature in momentum space as expected (see section 2.2.1). To see this, consider the Fourier transform of the superconducting gap

$$\Delta(\mathbf{k}) = \sum_{i=1}^{4}\Delta(\mathbf{d}_i)e^{i\mathbf{k}\cdot\mathbf{d}_i}, \tag{3.74}$$

[1]Here, it was used that $\chi(\mathbf{k})$ is symmetric in $\mathbf{k}$.

where one has that $\Delta(\mathbf{d}_{1,3}) = -\Delta(\mathbf{d}_{2,4}) \equiv -\,\Delta_0/2$ and the $\mathbf{k}$-vector has its components along the original lattice's $\mathbf{X}$- and $\mathbf{Y}$-directions. Therefore, using the expressions from equations (3.41-3.44), one gets

$$\begin{aligned}\Delta(\mathbf{k}) &= \Delta_0 \left(\cos\frac{(k_x + k_y)a}{2} - \cos\frac{(k_x - k_y)a}{2} \right) \\ &= \Delta_0 \left(\cos\frac{(k_x + k_y)a'}{\sqrt{2}} - \cos\frac{(k_x - k_y)a'}{\sqrt{2}} \right),\end{aligned} \tag{3.75}$$

where a is the lattice spacing between the copper atoms and $a' = a/\sqrt{2}$ is the spacing between the oxygen atoms. Comparing this with equation (2.46) shows that the superconducting order parameter has the same d-wave symmetry.

3.2.2 Critical temperature for $\mathbf{La_{2\text{-}x}Sr_xCuO_4}$

The actual number of holes in the system depends on the doping percentage. However, this relation is not a linear one, and may not even be known exactly [60]. For now, it will be described by the doping function $d(x)$. The relation can be entered in the partition function through a Lagrangian constraint

$$\lambda \left(N d(x) - \sum_{p=1}^{N} \sum_{C=A,B} \sum_{\sigma} \psi^{\dagger}_{C,\sigma,p} \psi_{C,\sigma,p} \right), \tag{3.76}$$

where N is the number of oxygen planes between two spacer layers and the constraint is enforced by including an integration over the multiplier field λ, which has as vacuum expectation value the chemical potential, $\langle \lambda \rangle = \mu$. The partition function of the effecitve Hamiltonian of equation (3.71), including the constraint, becomes

$$\mathcal{Z} = \frac{1}{\mathcal{Z}_0} \int \mathrm{D}\Psi \mathrm{D}\Delta \mathrm{D}M \mathrm{D}\lambda \, e^{-\iint \left[-\frac{|\Delta|^2}{g_S} - \frac{|M|^2}{g_P} - \lambda N d(x) + \Psi^{\dagger}(i\partial_\tau - \mathcal{H} + \lambda \tilde{I})\Psi \right] \mathrm{d}^2\mathbf{r}\mathrm{d}\tau}, \tag{3.77}$$

where $\mathcal{Z}_0$ is a normalization constant and $\tilde{I}$ corresponds to the the matrix with $(1, 1, -1, -1)$ on its diagonal. Expanding the imaginary time as a Matsubara sum, taking the mean-field approximation for the multiplier field and integrating over the Nambu fields leads to

$$\mathcal{Z} \propto \int \mathrm{D}\Delta \mathrm{D}M \mathrm{D}\mu \, e^{\iint V_{eff} \mathrm{d}^2\mathbf{r}\mathrm{d}\tau} \tag{3.78}$$

with the effective potential given by

$$\begin{aligned}V_{eff}\left[\Delta, M, \mu\right] =& \frac{|\Delta|^2}{g_S} + \frac{|M|^2}{g_P} + N\mu d(x) \\ &- \frac{N}{\beta} \sum_{n=-\infty}^{\infty} \sum_{l=\pm 1} \int \frac{\mathrm{d}^2 k}{4\pi^2} \ln \left[\omega_n^2 + \left(\sqrt{\epsilon^2(\mathbf{k}) + |M(\mathbf{k})|^2} + l\mu \right)^2 + |\Delta(\mathbf{k})|^2 \right].\end{aligned} \tag{3.79}$$

Minimizing the effective potential with respect to the different fields yields three conditions:

$$2|\Delta|\left(\frac{1}{g_S}-NT\sum_{n=-\infty}^{\infty}\sum_{l=\pm1}\int\frac{\mathrm{d}^2\mathbf{k}}{(2\pi)^2}\frac{1}{\omega_n^2+\left(\sqrt{\epsilon^2(\mathbf{k})+|M(\mathbf{k})|^2}+l\mu\right)^2+|\Delta|^2}\right)=0 \tag{3.80}$$

$$2|M|\left(\frac{1}{g_P}-NT\sum_{n=-\infty}^{\infty}\sum_{l=\pm1}\int\frac{\mathrm{d}^2\mathbf{k}}{(2\pi)^2}\frac{1+l\mu/\sqrt{\epsilon^2+|M(\mathbf{k})|^2}}{\omega_n^2+\left(\sqrt{\epsilon^2(\mathbf{k})+M^2}+l\mu\right)^2+|\Delta|^2}\right)=0 \tag{3.81}$$

$$Nd(x)-NT\sum_{n=-\infty}^{\infty}\sum_{l=\pm1}\int\frac{\mathrm{d}^2\mathbf{k}}{4\pi^2}\frac{2l\left(\sqrt{\epsilon^2(\mathbf{k})+|M(\mathbf{k})|^2}+l\mu\right)}{\omega_n^2+\left(\sqrt{\epsilon^2(\mathbf{k})+|M(\mathbf{k})|^2}+l\mu\right)^2+|\Delta(\mathbf{k})|^2}=0. \tag{3.82}$$

The critical temperature for the superconducting phase follows from the minimization equation for the superconducting gap in the limit that $M=0$ and $\Delta\to0$, see Appendix A. It is determined by the transcendental equation

$$T_c(x)=\frac{\alpha\eta(Ng_S)/2g_c}{\ln2+\ln\cosh\left[\mu(x)/2T_c(x)\right]}, \tag{3.83}$$

where $\eta(Ng)=(Ng-g_c)/Ng$ and $g_c=\alpha/\Lambda$ is a critical coupling parameter, which depends on α, a function of the characteristic velocity, and Λ, the characteristic energy scale related to the coherence length of the system. The maximum of the critical temperature $T_{c,max}=T_c(x_0)$ at the optimal doping level x_0 occurs for $\mu(x_0)=0$. In terms of the system's parameters it is given by

$$T_{c,max}=\frac{\Lambda}{2\ln2}\eta(Ng_S). \tag{3.84}$$

Compared to the conventional critical temperature from BCS theory (see equation (2.39)), one can see that both depend on the typical energy scale of the system and both are monotonically increasing functions of the coupling parameter. Substituting the expression for the maximum critical temperature into equation (3.83) leads to

$$\begin{aligned}T_c(x)&=\frac{T_{c,max}\ln2}{\ln2+\mu/2T_c+\ln\left(1+e^{-\mu/T_c}/2\right)}\\&\approx\frac{T_{c,max}\ln2}{\ln2+\mu/2T_c+(e^{-\mu/T_c}-1)/2},\end{aligned} \tag{3.85}$$

where on the right-hand side $\mu(x)$ and $T_c(x)$ are still functions of the doping concentration.

From the condition that $\mu(x_0)=0$, one can also gain some insight into the chemical potential. Namely, by combining the minimizations of the effective potential with respect to Δ and μ, as

shown in Appendix A, one finds that

$$\mu(x) = d(x)\frac{g_c}{2\eta(Ng_S)}. \tag{3.86}$$

In the case of a single spacer layer between the copper-oxygen planes (as one has for $La_{2-x}Sr_xCuO_4$), the simplest function for the hole concentration $d(x)$ that satisfies the two conditions, namely that $d(0) = 2$, the number of holes per area of the oxygen lattice's unit cell $A = a'^2$, and $d(x_0) = 0$, is $d(x) = 2|x_0 - x|/x_0$. This gives for the chemical potential

$$\mu(x) = 2\gamma(g_S)|x_0 - x|, \tag{3.87}$$

where $\gamma(g_S) = g_c/2x_0\eta(g_S)$. Substituting this chemical potential into equation (3.83) and taking the limit $T_c(x) \to 0$ gives the lowest and highest doping points at which the dome of the superconducting phase ends, namely

$$x_{sc,-} = x_0 - \frac{T_{c,max}}{\gamma}\ln 2, \tag{3.88}$$

$$x_{sc,+} = x_0 + \frac{T_{c,max}}{\gamma}\ln 2. \tag{3.89}$$

To conclude, equation (3.83) describes the symmetric superconducting dome in the phase diagram for $La_{2-x}Sr_xCuO_4$, which is bounded by the doping concentrations (3.88) and (3.89) and has a peak at the optimal doping level at height $T_{c,max} = \frac{\Lambda}{2\ln 2}\eta(Ng_S)$, see figure 3.6. This description of the superconducting phase will be used in the next chapter to investigate the influence of zinc impurities.

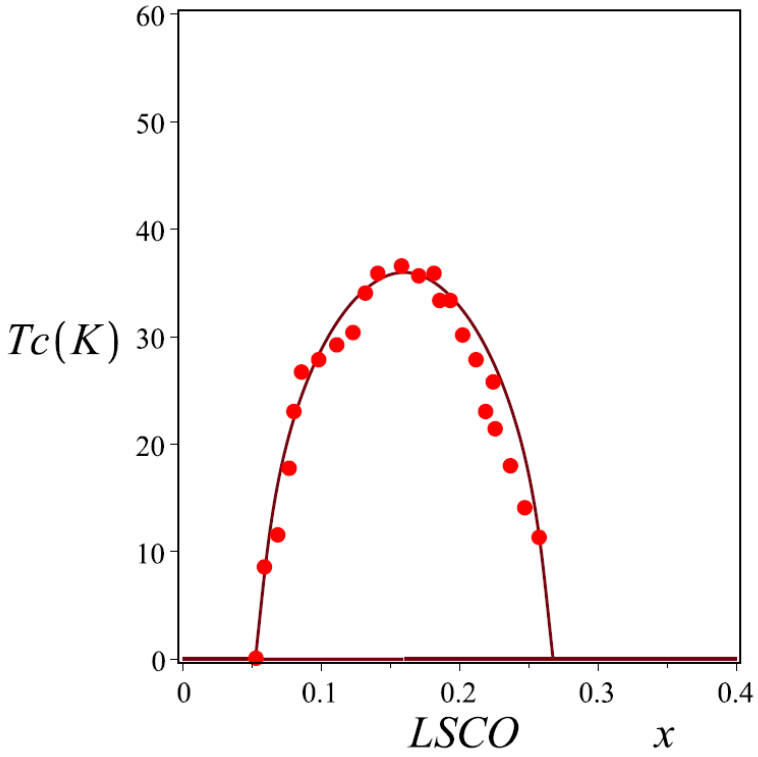

Figure 3.6: The dependence of the critical temperature on the doping concentration of strontium with data from experiments (the red circles) compared to the theory, taken from Ref. [60].

Chapter 4

Description of co-doped $La_{2-x}Sr_xCu_{1-z}Zn_zO_4$

In the previous chapter, the description of the effect of two types of doping into the LaCuO compound were given. One is the hole doping from replacing lanthanum with strontium, which leads to the superconducting phase at sufficiently high concentrations. The other is the impurity doping by zinc, which by replacing the copper atoms destroys the antiferromagnetic ordering of the copper-oxygen planes. In this chapter, the influence of the two dopants combined will be studied. In a previous work [49], the effect of co-doping on the Néel temperature and the antiferromagnetic ground state was investigated. The Néel temperature as a function of the zinc concentration z, $T_N(z)$, slightly increases before decreasing for low strontium doping [62]. As a function of hole doping x, the Néel temperature $T_N(x)$ decreases more slowly for higher zinc concentrations. These behaviours have been described in Ref. [55], for example.

In this thesis, the focus is on the effect of the zinc concentration z on the critical temperature T_c of the superconducting phase. The exchange of the copper ions with other transition elements like zinc is known to destroy the superconducting phase [51], which could give an insight into the mechanism underlying superconductivity in cuprates. The effect of the zinc doping on the critical temperature for the superconducting phase is even stronger than the effect on the Néel temperature, as small concentrations of only about 6% in YBCO [63] or $2-3\%$ in the underdoped regime of $La_{2-x}Sr_xCuO_4$ [64] suffice to completely suppress superconductivity.

Several of the dopants, either magnetic or nonmagnetic and with different valences, commonly investigated are nickel (valence 2+ with $S = 1$) [65], magnesium (valence 2+ with $S = 0$) [50], zinc (valence 2+ with $S = 0$), iron (valence 3+ and in high spin state), cobalt (valence 3+ and in low spin state), gallium (valence 3+ with $S = 0$) or aluminium (valence 3+ with $S = 0$) [51]. The advantage of zinc is that it has the same preferred valence state as copper (both are 2+), so the doping does not change the charge balance [66]. It also has a similar ionic radius, conserving the structure of the copper-oxygen planes as it replaces the copper ions. The main difference with the replaced copper ions is the nonmagnetic nature of zinc, due to the absence

of the spin-1/2 hole. The nonmagnetic zinc is known to be more effective at destroying the superconducting state than for example nickel ($S = 1$) [51], though magnesium ($S = 0$) seems to be similarly effective [50]. In conventional superconductors, nonmagnetic impurities barely affect the critical temperature [67], so this doping seems to directly influence the characteristic nature of high-temperature superconductivity.

4.1 Literature overview

In this section, an overview of some experimental results and proposed theoretical descriptions concerning the co-doping of LaCuO will be given. For the suppression of the superconducting critical temperature as a function of zinc doping, there are several groups of models [64]:

1. models treating the breaking of Cooper pairs caused by disorder or scattering, analogously to conventional superconductors with impurities,

2. models describing the superconducting-insulator transition from the perspective of a direct increase in resistance due to the zinc substitution,

3. models based on the superfluid picture, in which superconductivity is locally destroyed around each zinc impurity ("swiss cheese" model),

4. models focusing on stripes, that become pinned by the zinc impurities, and where the pinning of the stripes competes with the superconductivity.

In the first approach, BCS theory is adjusted by turning the interaction potential into a d-wave interaction [68]. The disorder from impurities is handled by adding a potential scattering or a magnetic Hamiltonian term to the standard H_{BCS}. One rather old theoretical description resulting from this is the Abrikosov-Gorkov theory, which predicts a universal behaviour following [69]

$$\ln \frac{T_c(z)}{T_c(0)} = \psi(1/2) - \psi\left(1/2 + 0.140z \frac{T_c(0)}{z_c T_c(z)}\right), \tag{4.1}$$

where $\psi(x) = \mathrm{d} \ln \Gamma(x)/\mathrm{d}x$ and z_c is the critical concentration at which $T_c(z)$ vanishes. The theory behind it is a pair-breaking mechanism due to the impurity's potential. Although the equation seems to fit to experiments in the low doping regime, where it becomes approximately linear, it does not work so well near the critical doping. Also, the universality or applicability of the relation to different compounds was questioned in Ref. [70], where instead a material dependent slope and a sudden drop near the critical concentration is predicted.

In the picture of the spin singlets, formed by the localized copper spins and the doped holes on the oxygen sites, it is assumed that the absence of the spin-1/2 hole on the zinc site leads to the breakdown of the singlet pairs, which gives rise to the suppression in the T_c [71]. The pair-breaking causes a decrease in the critical temperature as a function of zinc, which increases

with the strontium doping level at lower hole concentrations, i.e. the slope $|\mathrm{d}T_c/\mathrm{d}z|$ decreases as x increases. This dependence on the hole doping of the suppression rate of T_c was also found in Ref. [72], where measurements show that $T_c(z)$ has a roughly linear decrease. A linear decrease with the dopant concentration also shows up for elements other than zinc [51], see figure 4.1. For zinc, the linear decrease is higher for the underdoped regime [72]. The explanation for the difference between the underdoped and overdoped regimes given is again the picture of a zinc ion breaking a Cooper pair. However, the dependence of $|\mathrm{d}T_c/\mathrm{d}z|$ on the hole concentration was also linked to the evolution of the pseudogap in the underdoped regime. This link will be discussed in more detail further on.

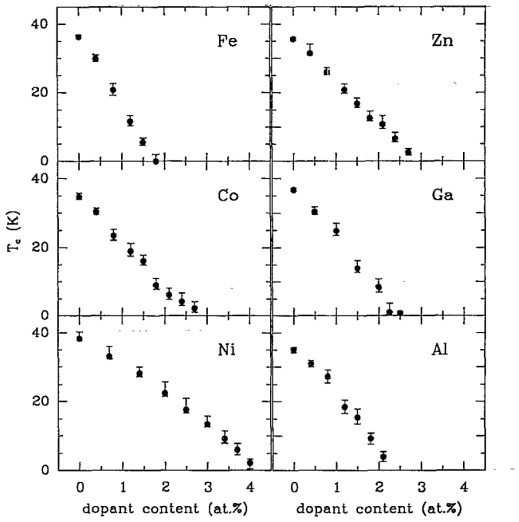

Figure 4.1: The critical temperature as a function of the dopant concentration for several elements [51]. All of these replace the copper atoms in $La_{1.85}Sr_{0.15}CuO_4$.

Some issues with these theories of pair-breaking due to a scattering potential are that they are mostly based on BCS theory and that they treat zinc as a purely nonmagnetic impurity, giving rise to only the potential scattering term, even though experiments have shown that zinc induces a magnetic moment in the Cu-O planes [51]. Also, in Ref. [73] it is stated that the pair-breaking models are insufficient in explaining the results, while the "swiss cheese" model of the third point can explain the dependence of T_c and the superfluid properties on the zinc concentration more accurately.

The second approach partially goes into the first as well, but here the assumption is that a loss of the superconductivity's coherence around the nonmagnetic impurities gives rise to a residual resistance [74]. This residual resistance is fairly large in the underdoped regime, but becomes quickly reduced in the overdoped regime [75]. The critical temperature as a function of this residual resistance forms a single pair-breaking curve in the underdoped regime, with a universal $\rho(T_c \to 0) \approx h/4e^2$, see figure 4.2. This residual resistance of $h/4e^2$ is the sheet resistance of

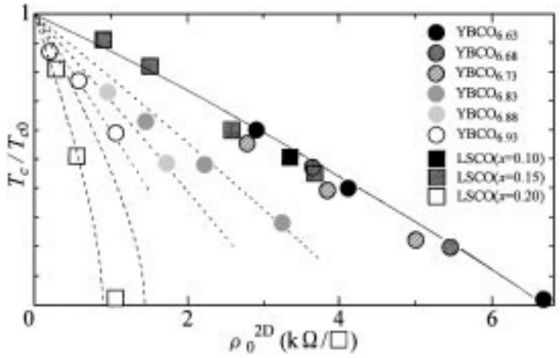

Figure 4.2: Renormalized critical temperature as a function of residual resistance caused by the zinc doping [75]. At lower hole doping levels, the curves collapse onto a universal line, while at higher levels the decrease is hole doping dependent.

the copper-oxygen planes [50]. The explanation for the appearance of the residual resistance is the so-called randomness effect that leads to the loss of the itinerant nature of the holes from the strontium doping. The randomness effect is the carrier localization by the disorder resulting from the zinc doping [71], which ties back to the disorder approach described above.

In the third approach, the "swiss cheese" model, the zinc impurity causes an area of roughly the square of the pair coherence length to be excluded from the superfluid state in the superconducting system [64]. This excluded area arises from a difference in the magnetic moment of the surrounding copper ions, even though zinc itself is nonmagnetic [76]. Namely, the localized spin-1/2s of the copper sites are no longer fully screened, resulting in a local moment on the zinc site. This localized magnetic moment has a magnitude of roughly one Bohr magneton ($1.0 - 1.2\mu_B$), corresponding to the copper's moment, which is usually concealed or screened, and decreases as more zinc is added [51]. As a result, the zinc impurity causes a scattering effect, which leads to a lower quasiparticle density in its vicinity [77]. The quasiparticle density is then linked to the effective moment at the zinc site.

In Ref. [78], it was found that the magnetic moment P_{eff}^2/Zn can also decrease with increasing hole concentrations, in which case it falls quite sharply until the hole doping level $x \approx 0.19$ is reached and further overdoping does not change the Zn-induced magnetic behavior significantly, see figure 4.3. Experimental observations indicated that the pseudogap also vanishes at $x \approx 0.19$ for cuprates (see references in Ref. [78]). The link with the pseudogap is also mentioned in the group's later work [72], though there in the picture of the pair-breaking mechanism.

This connection to the pseudogap is also brought up in Ref. [79], where it was found as well that the suppression rate $|\mathrm{d}T_c/\mathrm{d}z|$ is independent of the hole doping on the overdoped side, while it decreases with the hole concentration in the underdoped regime. This difference between the two regimes leads to an asymmetric collapse of the superconducting dome, where the optimal hole doping shifts to higher concentrations as the peak moves to the right, see figure 4.4. The

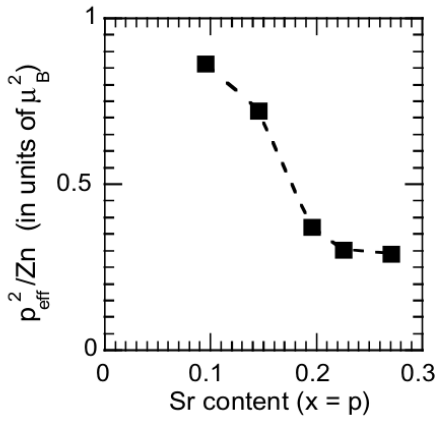

Figure 4.3: The effective magnetic moment P_{eff}^2/Zn as a function of the hole content for $La_{2-x}Sr_xCu_{1-y}Zn_yO_4$ [78].

explanation for this behaviour is based on the observation that the collapse of the dome appears to follow the "pseudogap line". Because of the opening of the pseudogap, the density of states is suppressed near the Fermi energy, as the pseudogap competes with the superconducting gap. This changes the scattering rate, leading to the increased suppression of T_c.

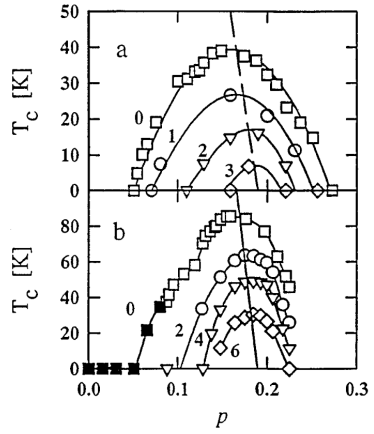

Figure 4.4: Critical temperature domes for different zinc doping levels [79]. The upper figure is for $La_{2-x}Sr_xCuO_4$, the lower figure for $YBa_2Cu_3O_{7-\delta}$. The pseudogap line indicated is from $YBa_2Cu_3O_{7-\delta}$, rescaled to the maximum temperature of $La_{2-x}Sr_xCuO_4$ in the upper figure.

The fourth approach is based on the stripes model, in which there is a separation between a spin-ordered phase and the superfluid [80]. The idea is then that the zinc impurities pin stripes and slow down their dynamics in a finite-size region around them. The effect is similar to the

"swiss cheese" model [80, 64] in that the superfluid density n_s is locally reduced. However, in Ref. [80], the zinc does not directly lessen the superfluid density, but instead increases the stripe effective mass density, yielding a decrease of $T_c \propto n_s/m$. From the connection of the effective mass to the kinetic energy density, which decreases with the zinc doping as the stripes become pinned, the ratio $T_c(x,z)/T_c(x,0) = 1 - z/z_c$ is found to describe the decrease of T_c with the zinc doping. Here, z_c is again the critical zinc concentration at which the critical temperature vanishes. In the underdoped regime, $z_c(x) \propto x^2$, while for optimal and overdoping, z_c is independent of the strontium concentration x. However, in Ref. [64] it is noted that this scaling of the critical zinc concentration $z_c \propto x^2$ is not necessarily compatible with results from Ref. [75], which indicate that the critical concentration is instead determined by the residual resistivity $\rho = (2h/\pi e^2)(z_c/x) = h/4e^2$, yielding $z_c \propto x$.

To emphasize, one of the most important phenomenological findings is that on the microscopic level, the zinc impurity causes an effective magnetic moment on surrounding copper sites [51]. That is, the magnetization becomes staggered around the zinc and so the antiferromagnetic correlations are locally enhanced [81, 76]. That zinc reveals the antiferromagnetic structure is also mentioned in Ref. [82], where it is furthermore claimed that the induced spins on the neighboring coppers are not correlated (which is a different picture from a single moment or spin cluster around the zinc impurity). The separate areas around the various zinc impurities are also barely interacting among each other [76].

Another important finding on a more macroscopic level, is that there is a universality for different compounds in that the suppression of the critical temperature as a function of zinc doping, $|\mathrm{d}T_c/\mathrm{d}z|$, is constant in the overdoped regime, but decreases with increasing hole concentration in the underdoped compounds, see also figure 4.5. The opposite happens with T_c as a function of the residual resistivity, where the curves collapse in the underdoped regime, but show a decreasing slope with increasing hole concentration in the overdoped regime [75].

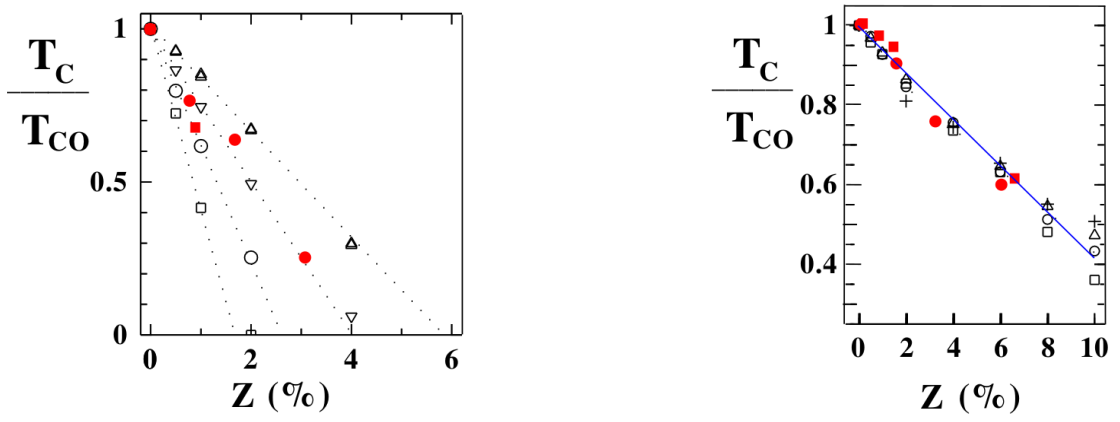

(a) (b)

Figure 4.5: The normalized critical temperature as a function of the zinc doping [80]. The red symbols correspond to Zn or Li doped $YBa_2Cu_3O_{7-x}$, the black symbols to Co doped $Bi_2Sr_2Ca_{1-y}Y_yCu_2O_{8+x}$. (a) Underdoped regime with different slopes for different hole doping levels. (b) Overdoped regime with universal behaviour for different hole doping levels.

4.2 Expanding the spin-fermion Hubbard model

The method that will be used in this work to describe the co-doping of La_2CuO_4 with strontium and zinc is based on the spin-fermion Hubbard model from Ref. [60] as described in section 3.2. The compound already contains the strontium ions, which cause the creation of Cooper pairs consisting of holes with a correlation length $\xi \approx 10$ Å [60], which is assumed to remain the same upon zinc doping.

In this section, the method and results for the inclusion of zinc doping into the spin-fermion Hubbard model will be presented. This is done by comparing the critical temperature as a function of the zinc concentration and the hole concentration from the strontium doping to experimental data from Refs [50, 51, 64, 72, 83].

A first assumption is that the zinc concentration z alters both the antiferromagnetic and the Kondo coupling strength J_{AF} and J_K. Namely, since the replacement with nonmagnetic zinc of a site in the antiferromagnetically ordered system changes the spin-based exchange locally, both the coupling J_{AF} with adjacent copper ions and the coupling with the itinerant holes at the surrounding oxygen sites J_K will be modified. As a result, the superconducting coupling g_S becomes a function of the zinc concentration, $g_S(z)$.

The goal is to determine the zinc dependence of the superconducting coupling by comparing the critical temperature to experimental data. Two different approaches for the incorporation of zinc through the superconducting coupling into the critical temperature will be investigated. The first takes the superconducting coupling as expected from percolation theory, the second assumes

that the superconducting coupling has a general linear dependence on the zinc concentration.

The critical temperature $T_c(x,z)$ is determined by equation (3.83) from chapter 3.2 (which for $La_{2-x}Sr_xCuO_4$ has $N=1$),

$$\begin{aligned} T_c(x,z) &= \frac{\frac{\alpha\eta}{2g_c}}{\ln 2 + \ln\cosh\frac{\mu_0(x)}{2T_c(x)}} \\ &= \frac{\Lambda(1-g_c/g_S(z))/2}{\ln 2\cosh\frac{\rho g_c(x_0-x)}{T_c(x,z)(1-g_c/g_S(z))}}, \end{aligned} \tag{4.2}$$

where $\eta = 1 - g_c/g_S$ and $\rho g_c/\eta = \rho g_c/(1-g_c/g_S) = \gamma$. The values of the parameters in this equation can be found in table 4.1. Note that the resulting critical temperature is in eV (1 eV $\sim$ 11604.5 K).

Λ (eV)	0.018
η	0.23870
γ (eV)	0.02
g_S (eV)	0.39406
g_c (eV)	0.3
ρ	0.016
x_0	0.16

Table 4.1: Values for the relevant parameters in the superconducting phase of $La_{2-x}Sr_xCuO_4$ [60].

Another way through which the zinc impurities might influence the system is the reduction of the kinetic energy around each zinc ion [80]. The kinetic energy enters as the hopping parameter t into the energy scale $\Lambda = 2\sqrt{2}\pi t a'/\xi$ and the critical coupling $g_c = 8\pi t^2/\Lambda = 2\sqrt{2}t\xi/a'$ [60]. The kinetic energy is assumed to be suppressed as $t(z) = t(1-z/z_c)$ [80]. The combination of this contribution with the superconducting coupling $g_S(z)$ results in the transcendental equation for the critical temperature

$$T_c = \frac{\Lambda\left(1-\frac{z}{z_c}\right)\left(1-\frac{g_c\left(1-\frac{z}{z_c}\right)}{g_S(z)}\right)/2}{\ln 2\cosh\frac{\rho(x_0-x)g_c\left(1-\frac{z}{z_c}\right)}{T_c\left(1-g_c\left(1-\frac{z}{z_c}\right)/g_S(z)\right)}}, \tag{4.3}$$

with the values for the parameters again given in table 4.1.

4.2.1 Percolation approach

In a first approach, the zinc dependence is taken from the percolation theory of Ref. [49], mentioned in chapter 3.1. The percolation factors change the Hamiltonian terms with localized spins, such

that

$$H_{AF} = J_{AF} K(z) \sum_{\langle I,\, J\rangle} \mathbf{S}_I \cdot \mathbf{S}_J, \tag{4.4}$$

$$H_K = J_K P_\infty(z) \sum_{I,\mathbf{R},\mathbf{d}_i} \mathbf{S}_I \cdot \big(\mathbf{S}_A(\mathbf{R}) + \mathbf{S}_B(\mathbf{R}+\mathbf{d}_i)\big), \tag{4.5}$$

where $P_\infty(z) = 1 - z$ is again the fraction of sites in the infinite cluster and $K(z) = 1 - 3z$ is the bond dilution factor. The percolation factors change the superconducting coupling constant as

$$g_S = \frac{J_K^2}{8J_{AF}} \to g_S(z) = \frac{J_K^2 P_\infty^2(z)}{8J_{AF}K(z)} = \frac{J_K^2(1-z)^2}{8J_{AF}(1-3z)}. \tag{4.6}$$

However, the function $P_\infty^2(z)/K(z) = (1-z)^2/(1-3z)$ increases with increasing z, so that this coupling increases with the zinc doping, see figure 4.6(a). As a result, the critical temperature $T_c(x,z) = T_c\left[g_S(z), \mu(x)\right]$ as a solution to equation (4.2) also increases, as shown in figure 4.6(b). Since it is expected that the superconductivity is suppressed, and it is known that the critical temperature decreases with increasing zinc doping, this approach seems implausible.

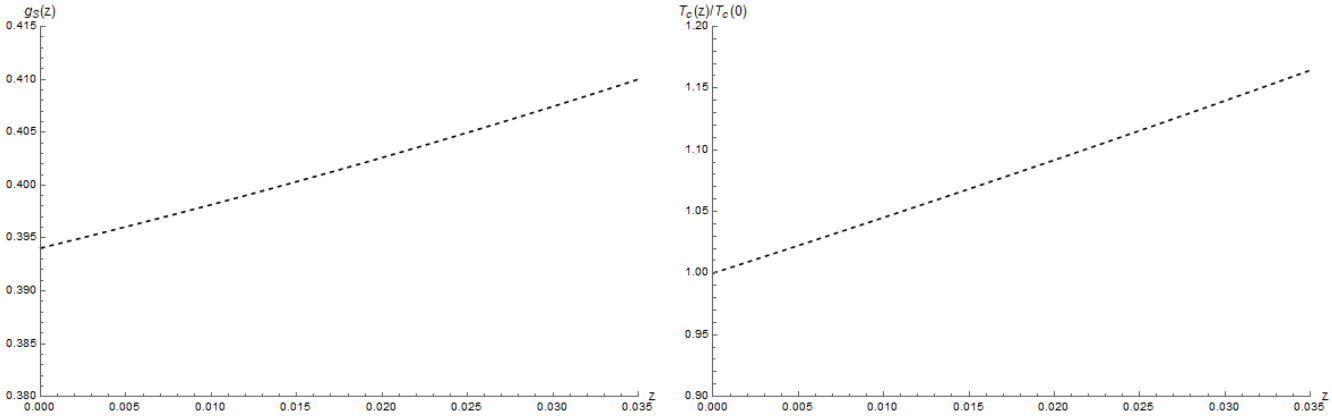

(a) (b)

Figure 4.6: The results from the percolation theory approach. (a) The superconducting coupling $g_S(z) = g_S(1-z)^2/(1-3z)$. (b) The resulting critical temperature $T_c(z)$ for $x = 0.1$, normalized with respect to $T_c(z=0)$.

Even with the inclusion of the zinc dependence of the kinetic energy, the percolation theory approach fails to describe the decreasing critical temperature, see figure 4.7. Therefore, it will be shown in the next subsection that the more general zinc dependence of the superconducting coupling provides a better description of the system.

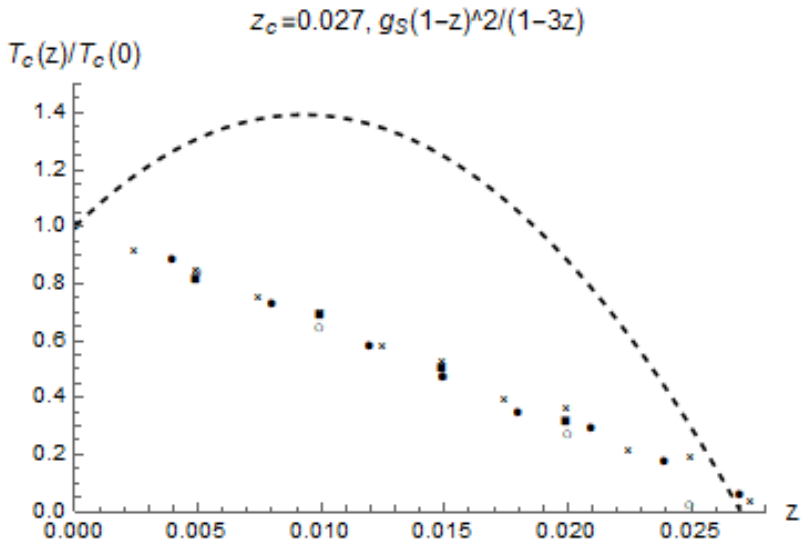

Figure 4.7: The normalized critical temperature $T_c(z)/T_c(z=0)$ for $x = 0.15$ with $g_S(z) = g_S(1-z)^2/(1-3z)$ and the kinetic energy dependence in $g_c(z)$ and $\Lambda(z)$, compared to experimental data (∘ Ref. [50], • Ref. [51], × Ref. [64], ■ Ref. [72]). The critical zinc concentration from experiments is $z_c = 0.027$.

4.2.2 General linear expansion

In this second approach, a more general expression for the superconducting coupling is used. Alternatively to the percolation approach, the reduction of the coupling constant can be described by an expansion in the zinc concentration z. The goal is then to fit the parameter b in the superconducting coupling constant

$$g_S(z) = g_S\,(1 - bz) \tag{4.7}$$

to the experimental data. Since the zinc concentration is small (less than 0.04 [64]), the expansion is only performed to first order. The parameter b for this linear dependence is determined from fitting the solution $T_c(x,z)/T_c(x,z=0)$ of equation (4.2) to the experimental data. This is done for the different strontium concentrations of $x = 0.10$, $x = 0.15$ and $x = 0.20$, each of which give an optimal b, see figure 4.8. For small zinc concentrations, the critical temperature from this approach seems to follow the data well, but at higher amounts of zinc doping, the ln cosh-term becomes more important and the theoretical function deviates from the experimental data.

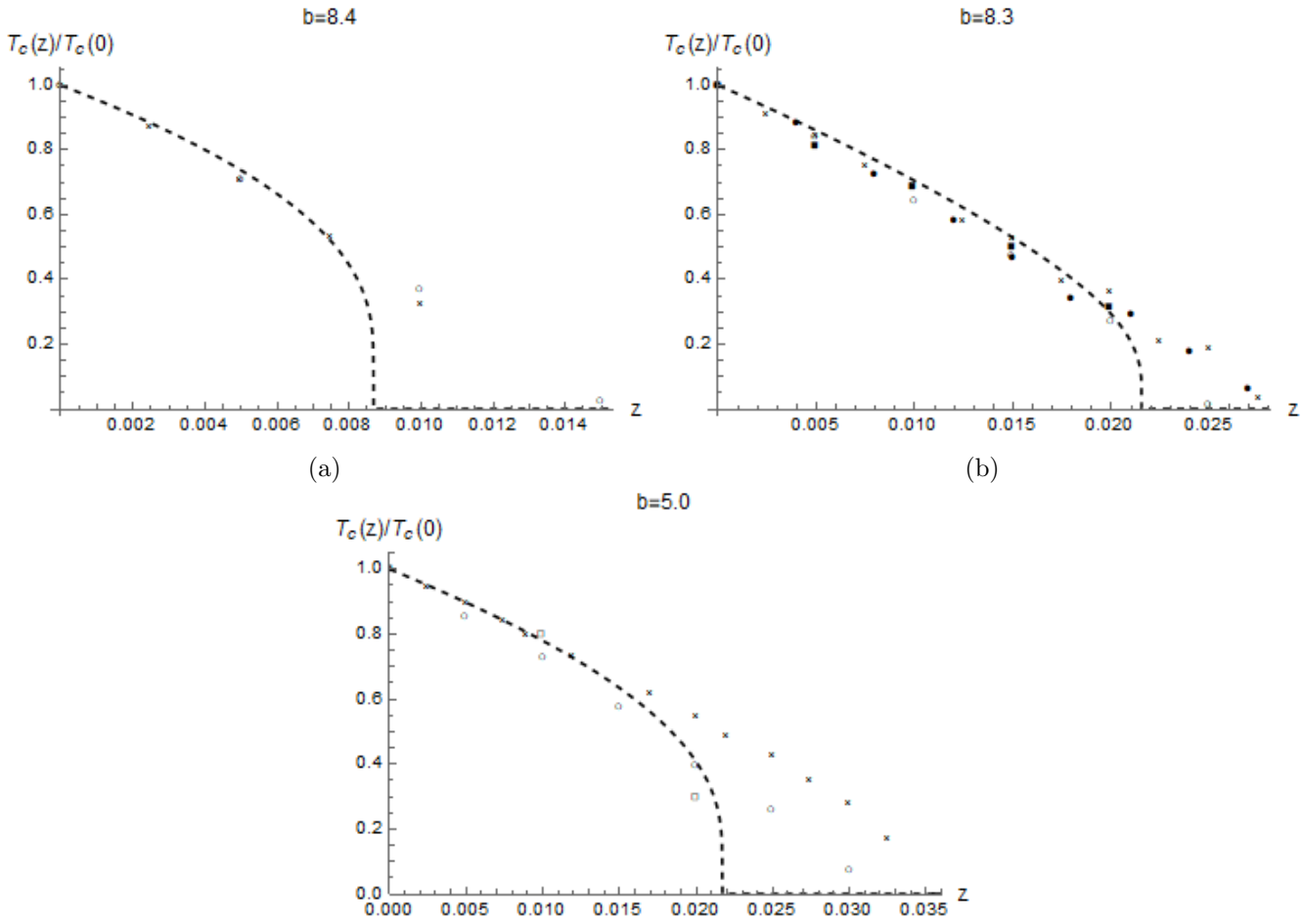

Figure 4.8: The normalized critical temperature $T_c(z)/T_c(z=0)$ for (a) $x = 0.10$, (b) $x = 0.15$ and (c) $x = 0.20$ with $g_S(z) = g_S(1 - bz)$, compared to experimental data (∘ Ref. [50], • Ref. [51], × Ref. [64], ■ Ref. [72], □ Ref. [83]). The optimal values for the linear parameter b found from fitting are indicated in the titles.

As mentioned before, the critical temperature can depend on the zinc concentration not only via the superconducting coupling, but also through the kinetic energy, as shown in equation (4.3). In this case, optimal values for both the linear parameter b as well as the critical zinc concentration z_c are found from fitting the normalized $T_c(z)$ to the experimental data for the different strontium concentrations of $x = 0.10$, $x = 0.15$ and $x = 0.20$. The results are shown in figure 4.9 and table 4.2. This fit returns values for z_c which are very close to a linear fit from the experimental data and the b-parameter equals $1/z_c$. Also noteworthy is that the critical zinc concentration increases almost linearly with the hole doping.

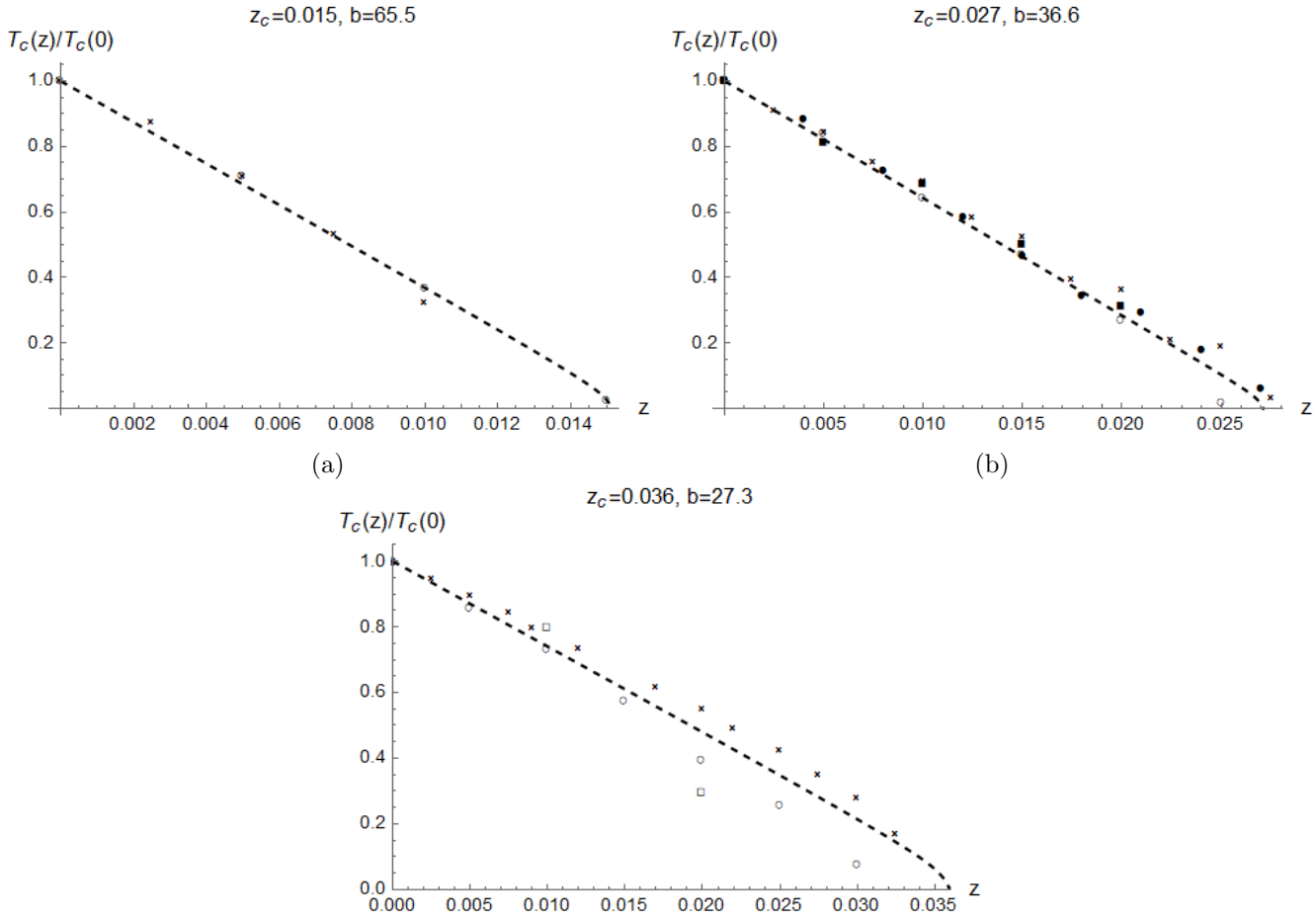

Figure 4.9: The normalized critical temperature $T_c(z)/T_c(z=0)$ for (a) $x = 0.10$, (b) $x = 0.15$ and (c) $x = 0.20$ with $g_S(z) = g_S(1-bz)$ and the kinetic energy dependence in $g_c(z)$ and $\Lambda(z)$, compared to experimental data (∘ Ref. [50], • Ref. [51], × Ref. [64], ■ Ref. [72], □ Ref. [83]). The optimal values for the critical zinc concentration z_c and the linear parameter b found from fitting are indicated in the titles. See also table 4.2.

x	b	$1/b$	z_c
0.10	65.5	0.0153	0.015
0.15	36.6	0.0274	0.027
0.20	27.3	0.0366	0.036

Table 4.2: The values for the linear parameter of $g_S(z) = g_S(1 - bz)$ and the critical zinc concentration z_c found from fitting the critical temperature of equation (4.3) to experimental data for different amounts of strontium doping x.

As a result, both the critical coupling and the superconducting coupling go with the zinc concentration as $(1 - z/z_c)$, such that the z-dependence of $\eta = 1 - g_c(z)/g_S(z)$ disappears and equation (4.3) reduces to

$$2T_c - \frac{\Lambda\left(1-\frac{z}{z_c}\right)\left(1-\frac{g_c}{g_S}\right)}{\ln 2\cosh\frac{\rho(x_0-x)\left(g_c\left(1-\frac{z}{z_c}\right)\right)}{T_c\left(1-\frac{g_c}{g_S}\right)}} = 0. \tag{4.8}$$

See figure 4.10 for the comparison of the critical temperature from this equation to the experimental data. Here, no fitting parameters are used, since the critical zinc concentration can be extracted from experiments.

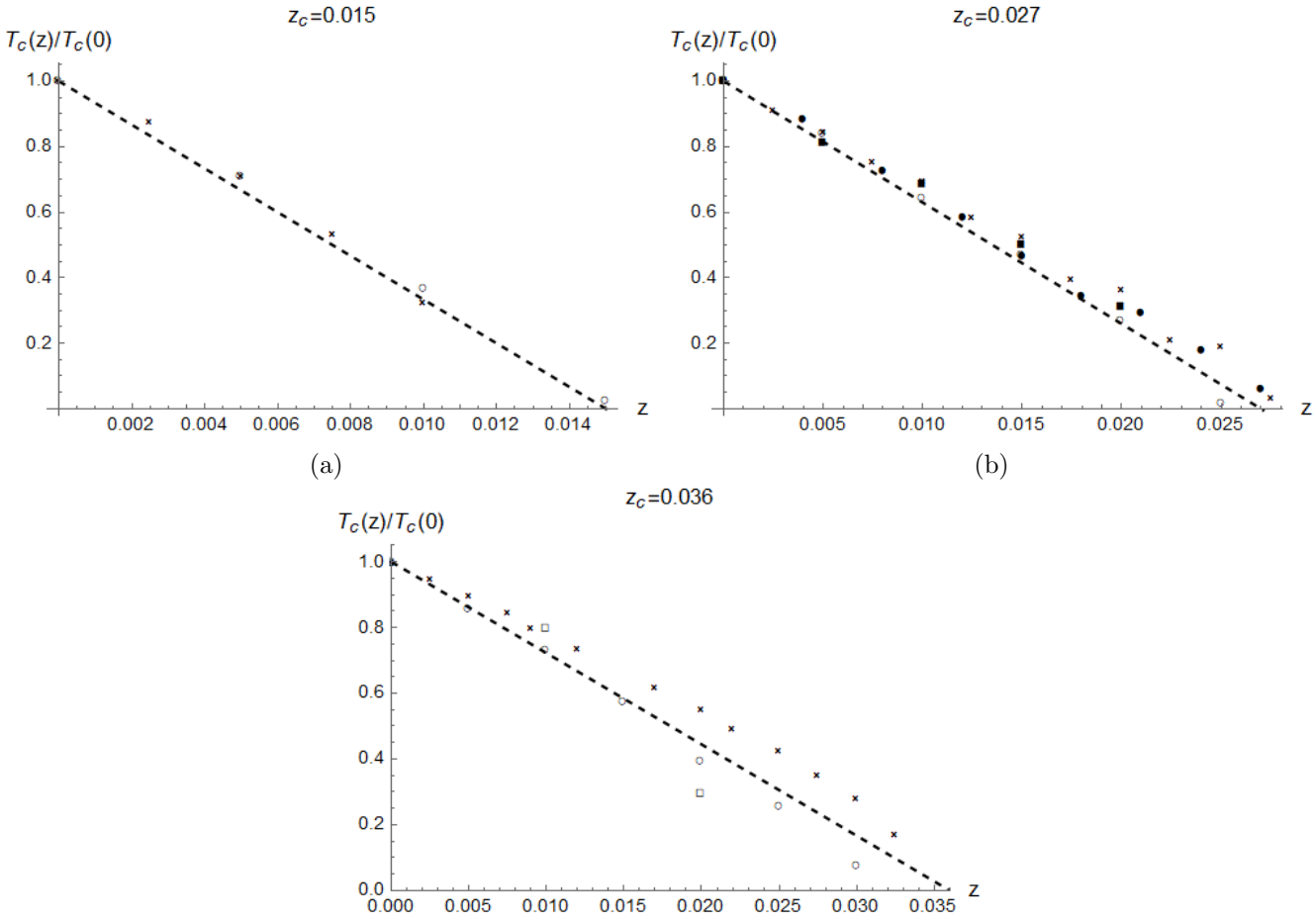

Figure 4.10: The normalized critical temperature $T_c(z)/T_c(0)$ for (a) $x = 0.10$, (b) $x = 0.15$ and (c) $x = 0.20$ using equation (4.8) with fixed z_c, compared to experimental data (○ Ref. [50], • Ref. [51], × Ref. [64], ■ Ref. [72], □ Ref. [83]).

This approach can be applied to other materials as well. Using equation (4.8) for $Bi_2Sr_2Ca(Cu_{1-z}Zn_z)_2O_{8+\delta}$ (Bi2212), for example, results in

$$T_c(x,z) - \frac{T_c^{max}\left(1-\frac{z}{z_c}\right)\ln 2}{\ln 2\cosh\frac{\rho(x_0-x)\left(g_c\left(1-\frac{z}{z_c}\right)\right)}{T_c\left(1-\frac{g_c}{2g_S}\right)}} \tag{4.9}$$

where $g_S \to 2g_S$, to account for the two copper-oxygen planes, $T_c^{max} = \Lambda/2\ln 2$ and the parameters are as given in table 4.3. Note that this equation only holds in the underdoped regime, since the superconducting dome of Bi2212 is asymmetric around the optimal doping point [60]. In the overdoped regime, the transcendental equation becomes

$$T_c(x,z) - \frac{T_c^{max}\left(1-\frac{z}{z_c}\right)\ln 2}{\ln\left(1+e^{-\gamma(x_0-x)(1-z/z_c)/T_c}\right)} = 0. \tag{4.10}$$

Using the critical zinc concentration found from a fitting to the data from Ref. [84] gives the plots shown in figure 4.11.

T_c^{max} (eV)	0.0080
η	0.61538
γ (eV)	0.041
g_S (eV)	0.3900
g_c (eV)	0.3
x_0	0.245

Table 4.3: Values for the relevant parameters in the superconducting phase of the bilayer $Bi_2Sr_2CaCu_2O_{8+\delta}$ [60].

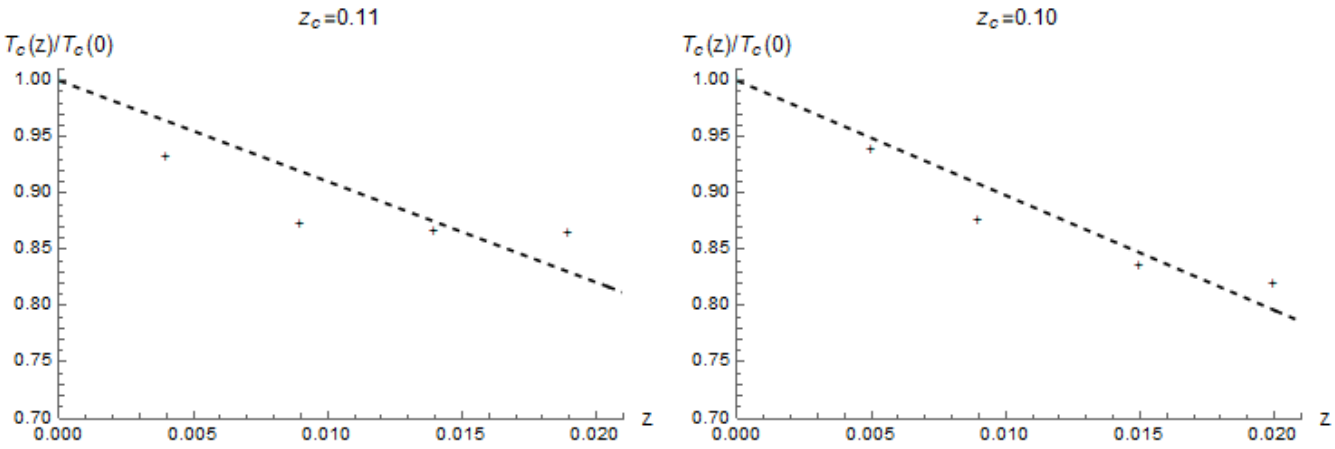

(a) (b)

Figure 4.11: Plot of $T_c(z)/T_c(z = 0)$ given by (a) equation (4.9) for $x = 0.19$ (underdoped regime) and (b) equation (4.10) for $x = 0.25$ (overdoped regime), both with the parameters from table 4.3 for $Bi_2Sr_2Ca(Cu_{1-z}Zn_z)_2O_{8+x}$ compared to the experimental data of Ref. [84]. The values of the critical zinc concentration z_c from fitting are given on top of each plot.

4.2.3 Summary

The main result from the expansion of the spin-fermion Hubbard model to the co-doped $La_{2-x}Sr_x$-$Cu_{1-z}Zn_zO_4$ system is the dependence of the superconducting coupling constant, the critical coupling, and the energy scale on the zinc doping amount z and the critical concentration z_c as $(1 - z/z_c)$. As a consequence, the critical temperature $T_c(x, z)$ for the superconducting phase is the solution to the equation

$$T_c(x,z) - \frac{\Lambda\left(1-\frac{z}{z_c}\right)\left(1-\frac{g_c}{g_S}\right)/2}{\ln 2\cosh\frac{\rho(x_0-x)\left(g_c\left(1-\frac{z}{z_c}\right)\right)}{T_c(x,z)\left(1-\frac{g_c}{g_S}\right)}} = 0, \tag{4.11}$$

since the zinc dependence from the critical coupling and the superconducting coupling cancel out.

4.3 Discussion

In the first trial approach to the inclusion of zinc, the nonmagnetic impurity was treated as an exclusively on-site effect, removing a single spin site from the antiferromagnetic copper lattice that is the background for the itinerant holes in the spin-fermion Hubbard model. This effect was included through percolation theory as introduced by Ref. [49], where it had successfully described the destruction of the Néel state, both in the purely zinc doped and the co-doped compounds.

However, in the superconducting system, this approach is insufficient to explain the destruction of superconductivity upon zinc doping. Even with inclusion of the kinetic energy suppression as proposed in Ref. [80], the superconducting coupling following from percolation theory does not give the correct reduction in the critical temperature.

Instead, fitting of the experimental data with a single fitting parameter shows that the superconducting coupling goes with $(1 - z/z_c)$, the same dependence as the kinetic energy. The contribution to the kinetic energy comes from the picture in which each zinc impurity perturbs the magnetization in a finite area around it, thereby disrupting the hopping of the charge carriers ("swiss cheese" model) [80]. Since the contribution to the superconducting coupling is the same, it can be assumed that this as well is affected by the same excluded area, not only through the local spin change. This means that the Cooper pairs are limited in their coherent movement by the zinc impurities.

The inclusion of the kinetic energy reduction is necessary to explain the data. It gives most of the linear behaviour in the zinc concentration of the critical temperature in the regime where the $\ln\cosh$-term plays a large role, i.e. near the critical zinc concentration. Note that this is different from Ref. [80], where $T_c(z)$ decreases linearly precisely with the same dependence as the kinetic energy in the entire regime. A byproduct of the inclusion of the kinetic energy dependence is that the ratio of the couplings g_c/g_S and as a result $\eta = 1 - g_c/g_S$ remain the same upon zinc doping.

For Bi2212, the theory does not fit the data so well in the underdoped regime, but slightly better just above the optimal doping level. It is interesting to note that the best fitting critical zinc concentrations are almost equal for the two cases. In the results for LSCO, the critical zinc concentration increases with increasing hole doping, in a way that it seems not to be universal in the optimal and overdoped regime. Rather, z_c increases almost linearly with the strontium doping. The critical zinc concentration can be seen as the amount of zinc necessary to have the areas where superconductivity is destroyed percolating through the system. An increase in z_c would indicate a decrease in the size of the affected region, which seems to occur for higher hole concentrations. It is in this picture of the "swiss cheese" model that the zinc impurity should be considered, especially since experiments show the induction of magnetic moments on copper sites surrounding the zinc impurities and an effective magnetic moment on the zinc ions themselves [51]. However, the linear increase of the critical zinc concentration with strontium doping in the optimal and overdoped regime is in disagreement with Ref. [80] (see figure 4.5b), but corresponds to the expectation of $z_c \propto x$ from Ref. [64]. More research is necessary to satisfactorily determine how the critical zinc concentration depends on the strontium doping.

All the results in this work are based upon the spin-fermion Hubbard model, which is a mean-field approximation used to describe the overall superconducting system. A more general approach would be needed to gain more insight into the microscopic features. Another product of this approach is the absolute separation between the pseudogap and superconducting phases. While from experiments it appears that the pseudogap might play a role in the underdoped regime [79], this effect is not included here. It might be that the exclusion of the pseudogap leads to the absence of a significant difference in the results between the underdoped and overdoped regime.

Chapter 5

Conclusion

In this work, the destruction of high-temperature superconductivity in cuprates through the doping of zinc as a nonmagnetic impurity was investigated, with the main focus on $La_{2-x}Sr_2CuO_4$. For this purpose, the spin-fermion Hubbard model as described in Ref. [60] for the superconducting system was extended to include doping by zinc. It was found that the zinc impurity not only affects the on-site spin of the antiferromagnetic background, but also the kinetic energy of the itinerant holes in its vicinity.

The effect of the impurity on a single spin was incorporated into the superconducting coupling through the percolation theory approach from Ref. [49]. However, this is not sufficient to explain the decrease in the critical temperature upon zinc doping. Rather, the superconducting coupling is suppressed with a linear term in the amount of zinc and the critical zinc concentration, at which both the superconducting coupling and the critical temperature vanish. This linear decrease with the zinc concentration was found to be the same as the dependence of the kinetic energy as proposed by Ref. [80].

Moreover, both contributions of zinc dependence in the critical temperature, namely from the kinetic energy and from the superconducting coupling, need to be considered to describe the experimental data satisfactorily. The zinc dependent kinetic energy enters into the hopping parameter of the itinerant holes between the oxygen sites and subsequently into the critical coupling strength and the energy scale of the superconductivity. The critical coupling gives the minimum value of the superconducting coupling for a phase transition to occur, while the energy scale determines the maximum value below which superconducting Cooper pairs can be considered [60].

This means that both the formation and the dynamics of Cooper pairs are affected in the same manner in a region surrounding the zinc impurities, the size of which decreases with increasing hole concentration. It would be interesting to find how the affected area around each zinc impurity precisely depends on the hole doping and how the suppression of the coupling and the kinetic energy works microscopically. Further research could also be done into the pseudogap and its interplay with the nonmagnetic zinc impurities.

Appendix A

Additional details on the minimization of the effective potential

In this section, the details on the minimization of the effective potential,

$$\begin{aligned} V_{eff}\left[\Delta, M, \mu\right] =& \frac{|\Delta|^2}{g_S} + \frac{|M|^2}{g_P} + N\mu d(x) \\ & - \frac{N}{\beta}\sum_{n=-\infty}^{\infty}\sum_{l=\pm 1}\int \frac{\mathrm{d}^2 k}{4\pi^2}\ln\left[\omega_n^2 + \left(\sqrt{\epsilon^2(\mathbf{k}) + |M(\mathbf{k})|^2} + l\mu\right)^2 + |\Delta(\mathbf{k})|^2\right], \end{aligned} \tag{A.1}$$

for the Spin-Fermion-Hubbard model from section 3.2 will be given.

Superconducting gap

Firstly, minimizing this potential with respect to the superconducting gap leads to

$$\frac{\delta V_{eff}}{\delta \Delta} = \frac{2|\Delta|}{g_S} - NT\sum_{l=\pm 1}\int \frac{\mathrm{d}^2\mathbf{k}}{(2\pi)^2}\sum_{n=-\infty}^{+\infty}\frac{2|\Delta|}{\omega_n^2 + \left(\sqrt{v^2\mathbf{k}^2 + M^2} + l\mu\right)^2 + \Delta_0^2} = 0. \tag{A.2}$$

This has as solutions that either $|\Delta| = 0$ or the difference between $1/g_S$ and the integral vanishes. This difference can be rewritten in the following way. First, the Matsubara sum can be evaluated through $\sum_{n=-\infty}^{+\infty} 1/(\omega_n^2 + \zeta^2) = 1/(2T\zeta)\tanh\left(\zeta/2T\right)$, such that the above equation becomes

$$\frac{1}{g_S} - N\sum_{l=\pm 1}\int \frac{\mathrm{d}^2\mathbf{k}}{(2\pi)^2}\frac{1}{2\sqrt{\left(\sqrt{v^2\mathbf{k}^2 + M^2} + l\mu\right)^2 + \Delta_0^2}}\tanh\left(\frac{\sqrt{\left(\sqrt{v^2\mathbf{k}^2 + M^2} + l\mu\right)^2 + \Delta^2}}{2T}\right) = 0. \tag{A.3}$$

Changing the integration variable $\mathbf{k}$ to $\epsilon = v^2\mathbf{k}^2$ turns the integral over $\int \mathrm{d}^2\mathbf{k}/(2\pi)^2 = \int k\,\mathrm{d}k/2\pi$ into an integral over $\int_0^{\Lambda^2} \mathrm{d}\epsilon/4\pi v^2 = \int_0^{\Lambda^2} \mathrm{d}\epsilon/2\alpha$, where Λ^2 is the energy cutoff of the Fermi level and $\alpha = 2\pi v^2$. The difference in equation (A.3) then becomes

$$\frac{1}{g_S} - \frac{N}{4\alpha}\sum_{l=\pm1}\int_0^{\Lambda^2} \frac{\mathrm{d}\epsilon}{\sqrt{\left(\sqrt{\epsilon+M^2}+l\mu\right)^2+\Delta^2}}\,\tanh\left(\frac{\sqrt{\left(\sqrt{\epsilon+M^2}+l\mu\right)^2+\Delta^2}}{2T}\right) = 0. \tag{A.4}$$

Changing again the integration variable from ϵ to $y_l(\epsilon) = \frac{1}{2T}\sqrt{\left(\sqrt{\epsilon+M^2}+l\mu\right)^2+\Delta^2}$ with

$$2T\,\mathrm{d}y_l = \frac{\sqrt{\epsilon+M^2}+l\mu}{\sqrt{\left(\sqrt{\epsilon+M^2}+l\mu\right)^2+\Delta^2}}\frac{\mathrm{d}\epsilon}{2\sqrt{\epsilon+M^2}}, \tag{A.5}$$

$$\sqrt{\epsilon+M^2} = \sqrt{(2Ty_l)^2-\Delta^2} - l\mu \tag{A.6}$$

results in

$$\begin{aligned}\frac{4\alpha}{Ng_S} - \sum_{l=\pm1}\int_{y_l(0)}^{y_l(\Lambda^2)} \frac{4T\sqrt{\epsilon+M^2}}{\sqrt{\epsilon+M^2}+l\mu}\tanh y_l\,\mathrm{d}y_l = \\ \frac{4\alpha}{Ng_S} - 4T\sum_{l=\pm1}\int_{y_l(0)}^{y_l(\Lambda^2)}\left[1-\frac{l\mu}{\sqrt{(2Ty_l)^2-\Delta^2}}\right]\tanh y_l\,\mathrm{d}y_l = 0.\end{aligned} \tag{A.7}$$

The first part of the integral gives

$$\int_{y_l(0)}^{y_l(\Lambda^2)} \tanh y_l\,\mathrm{d}y_l = \ln\cosh y_l(\Lambda^2) - \ln\cosh y_l(0), \tag{A.8}$$

while the second part is of the form

$$\int_{y_l(0)}^{y_l(\Lambda^2)} \frac{1}{\sqrt{y_l^2-D^2}}\tanh y_l\,\mathrm{d}y_l\,, \tag{A.9}$$

where $D = \Delta/2T$. In the limit $\Delta \to 0$, $T \to T_c$ ($M = 0$), this is an integral over $\tanh y/y$, which can be evaluated using the expansion $\tanh y = \sum_{n=1}^{\infty} 2^{2n}(2^{2n}-1)B_{2n}y^{2n-1}/(2n)!$, such that

$$\begin{aligned}\int_{y_l(0)}^{y_l(\Lambda^2)} \frac{1}{y_l}\tanh y_l\,\mathrm{d}y_l &= \sum_{n=1}^{\infty}\frac{2^{2n}(2^{2n}-1)B_{2n}}{(2n)!}\int_{y_l(0)}^{y_l(\Lambda^2)} y_l^{2n-2}\,\mathrm{d}y_l \\ &= \sum_{n=1}^{\infty}\frac{2^{2n}(2^{2n}-1)B_{2n}}{(2n)!}\frac{1}{2n-1}\left(\left[\frac{\Lambda+l\mu}{2T_c}\right]^{2n-1} - \left[\frac{l\mu}{2T_c}\right]^{2n-1}\right).\end{aligned} \tag{A.10}$$

Since $\Lambda \gg \mu$, the first term from the upper bound of the integral dominates and it is possible to expand in terms of μ/Λ, so that

$$\begin{aligned}
4T_c \sum_{l=\pm 1} l\mu \sum_{n=1}^{\infty} \frac{2^{2n}(2^{2n}-1)B_{2n}}{(2n)!} \frac{1}{2n-1} \left(\left[\frac{\Lambda + l\mu}{2T_c} \right]^{2n-1} - \left[\frac{l\mu}{2T_c} \right]^{2n-1} \right) \\
&\approx 4T_c\mu \sum_{l=\pm 1} \sum_{n=1}^{\infty} \frac{2^{2n}(2^{2n}-1)B_{2n}}{(2n)!} \frac{l}{2n-1} \left[\frac{\Lambda}{2T_c} \right]^{2n-1} \left(1 + (2n-1)\frac{l\mu}{\Lambda} \right) \\
&= 4T_c\mu \sum_{n=1}^{\infty} \frac{2^{2n}(2^{2n}-1)B_{2n}}{(2n)!} \frac{1}{2n-1} \left[\frac{\Lambda}{2T_c} \right]^{2n-1} \left(1 + (2n-1)\frac{\mu}{\Lambda} - \left[1 - (2n-1)\frac{\mu}{\Lambda} \right] \right) \\
&= 8T_c\mu \frac{\mu}{\Lambda} \sum_{n=1}^{\infty} \frac{2^{2n}(2^{2n}-1)B_{2n}}{(2n)!} \left[\frac{\Lambda}{2T_c} \right]^{2n-1} = 8T_c \frac{\mu^2}{\Lambda} \tanh \frac{\Lambda}{2T_c}.
\end{aligned} \tag{A.11}$$

As a result, equation (A.7) becomes

$$\frac{4\alpha}{Ng_S} - 4T_c \left(\ln\cosh \frac{\Lambda+\mu}{2T_c} + \ln\cosh \frac{\Lambda-\mu}{2T_c} - 2\ln\cosh \frac{\mu}{2T_c} \right) - 8T_c \frac{\mu^2}{\Lambda} \tanh \frac{\Lambda}{2T_c} = 0. \tag{A.12}$$

Rearranging and using again that $\Lambda \gg \mu$ leads to

$$\begin{aligned}
\frac{\alpha}{2Ng_ST_c} - \frac{\mu^2}{\Lambda} \tanh \frac{\Lambda}{2T_c} - \left(\ln\cosh \frac{\Lambda}{2T_c} - \ln\cosh \frac{\mu}{2T_c} \right) = 0 \\
\frac{\alpha}{2Ng_ST_c} \left(1 - \frac{2Ng_ST_c}{g_c} \frac{\mu^2}{\Lambda^2} \right) - \left(\ln\cosh \frac{\Lambda}{2T_c} - \ln\cosh \frac{\mu}{2T_c} \right) = 0,
\end{aligned} \tag{A.13}$$

where $g_c = \alpha/\Lambda$ is the critical coupling and the term with μ^2/Λ^2 can be neglected, leading to

$$\frac{\alpha}{2Ng_ST_c} - \left(\ln\cosh \frac{\Lambda}{2T_c} - \ln\cosh \frac{\mu}{2T_c} \right) = 0, \tag{A.14}$$

which is

$$\frac{\alpha}{2Ng_ST_c} = \ln \frac{\cosh \Lambda/2T_c}{\cosh \mu/2T_c}. \tag{A.15}$$

Taking the exponent on both sides and expanding $\cosh \Lambda/2T_c = e^{\Lambda/2T_c}(1 + e^{-\Lambda/T_c})/2$ gives

$$e^{-\alpha/2Ng_ST_c + \Lambda/2T_c} \left(1 + e^{-\Lambda/T_c} \right) = 2\cosh \frac{\mu}{2T_c} \tag{A.16}$$

$$e^{\Lambda(1-g_c/Ng_S)/2T_c} = \frac{2}{1+e^{-\Lambda/T_c}} \cosh \frac{\mu}{2T_c}. \tag{A.17}$$

Taking the natural logarithm of both sides and assuming that $\Lambda \gg T_c$, such that $e^{-\Lambda/T_c} \approx 0$ results in

$$\frac{\Lambda\eta}{2T_c} = \ln 2 + \ln\cosh\frac{\mu}{2T_c}, \tag{A.18}$$

where $\eta = 1 - g_c/Ng_S$. Rearranging for T_c on the left hand side of the equation results in the transcendental equation for the critical temperature as given in equation (3.83).

Something similar can be done for the pseudogap, but this will not be given in more detail here, as the focus of this work is on the superconducting gap.

Chemical potential

Minimizing the effective potential of equation (A.1) with respect to the chemical potential μ leads to

$$\frac{\delta V_{eff}}{\delta\mu} = Nd(x) - \frac{N}{\beta}\sum_{n=-\infty}^{\infty}\sum_{l=\pm1}\int\frac{\mathrm{d}^2\mathbf{k}}{4\pi^2}\frac{2l\left(\sqrt{\epsilon^2(\mathbf{k})+M^2}+l\mu\right)}{\omega_n^2+\left(\sqrt{\epsilon^2(\mathbf{k})+|M(\mathbf{k})|^2}+l\mu\right)^2+|\Delta(\mathbf{k})|^2} = 0. \tag{A.19}$$

After the evaluation of the Matsubara sum, this becomes

$$d(x) - \sum_{l=\pm1}\int\frac{\mathrm{d}^2\mathbf{k}}{4\pi^2}\frac{2l\left(\sqrt{v^2\mathbf{k}^2+|M(\mathbf{k})|^2}+l\mu\right)}{2\sqrt{\left(\sqrt{v^2\mathbf{k}^2+M^2}+l\mu\right)^2+\Delta^2}}\tanh\left(\frac{\sqrt{\left(\sqrt{v^2\mathbf{k}^2+M^2}+l\mu\right)^2+\Delta^2}}{2T}\right) = 0. \tag{A.20}$$

With the same substitution of $\epsilon = v^2\mathbf{k}^2$ and $y_l(\epsilon) = \frac{1}{2T}\sqrt{\left(\sqrt{\epsilon+M^2}+l\mu\right)^2+\Delta^2}$, this becomes

$$\begin{aligned} 2\alpha d(x) - \sum_{l=\pm1} l\int_0^{\Lambda^2}\frac{\left(\sqrt{\epsilon+M^2}+l\mu\right)\mathrm{d}\epsilon}{\sqrt{(\sqrt{\epsilon+M^2}+l\mu)^2+\Delta^2}}\tanh\frac{\sqrt{(\sqrt{\epsilon+M^2}+l\mu)^2+\Delta^2}}{2T} = \\ 2\alpha d(x) - 4T\sum_{l=\pm1} l\int_{y_l(0)}^{y_l(\Lambda^2)}\sqrt{\epsilon+M^2}\tanh y_l\,\mathrm{d}y_l = \\ 2\alpha d(x) - 4T\sum_{l=\pm1} l\int_{y_l(0)}^{y_l(\Lambda^2)}\left[\sqrt{(2Ty_l)^2-\Delta^2}-l\mu\right]\tanh y_l\,\mathrm{d}y_l = 0. \end{aligned} \tag{A.21}$$

The integral over $\mu\tanh y_l$ gives again the typical $\ln\cosh y_l$ terms. In the case that $\Delta \to 0$ and $T \to T_c$ ($M = 0$), the remaining integral is of the form

$$\int_{y_l(0)}^{y_l(\Lambda^2)} y_l\tanh y_l\,\mathrm{d}y_l\,. \tag{A.22}$$

This integral can be evaluated in the same manner as the integral for the minimization with respect to the superconducting gap in the previous subsection, i.e. by writing $\tanh y = \sum_{n=1}^{\infty} 2^{2n}(2^{2n}-1)B_{2n}y^{2n-1}/(2n)!$, such that

$$\begin{aligned}\int_{y_l(0)}^{y_l(\Lambda^2)} y_l \tanh y_l \, \mathrm{d}y_l &= \sum_{n=1}^{\infty} \frac{2^{2n}(2^{2n}-1)B_{2n}}{(2n)!} \int_{y_l(0)}^{y_l(\Lambda^2)} y_l^{2n} \, \mathrm{d}y_l \\ &= \sum_{n=1}^{\infty} \frac{2^{2n}(2^{2n}-1)B_{2n}}{(2n)!} \frac{1}{2n+1} \left(\left[\frac{\Lambda + l\mu}{2T_c} \right]^{2n+1} - \left[\frac{l\mu}{2T_c} \right]^{2n+1} \right).\end{aligned} \tag{A.23}$$

Since $\Lambda \gg \mu$, the first term from the upper bound of the integral dominates and it is possible to expand in terms of μ/Λ, so that

$$\begin{aligned}&8T_c^2 \sum_{l=\pm 1} l \sum_{n=1}^{\infty} \frac{2^{2n}(2^{2n}-1)B_{2n}}{(2n)!} \frac{1}{2n+1} \left(\left[\frac{\Lambda + l\mu}{2T_c} \right]^{2n+1} - \left[\frac{l\mu}{2T_c} \right]^{2n+1} \right) \\ &\quad \approx 8T_c^2 \sum_{l=\pm 1} \sum_{n=1}^{\infty} \frac{2^{2n}(2^{2n}-1)B_{2n}}{(2n)!} \frac{l}{2n+1} \left[\frac{\Lambda}{2T_c} \right]^{2n+1} \left(1 + (2n+1)\frac{l\mu}{\Lambda} \right) \\ &\quad = 8T_c^2 \sum_{n=1}^{\infty} \frac{2^{2n}(2^{2n}-1)B_{2n}}{(2n)!} \frac{1}{2n+1} \left[\frac{\Lambda}{2T_c} \right]^{2n+1} \left(1 + (2n+1)\frac{\mu}{\Lambda} - \left[1 - (2n+1)\frac{\mu}{\Lambda} \right] \right) \\ &\quad = 8T_c^2 \left(\frac{\Lambda}{2T_c} \right)^2 \frac{2\mu}{\Lambda} \sum_{n=1}^{\infty} \frac{2^{2n}(2^{2n}-1)B_{2n}}{(2n)!} \left[\frac{\Lambda}{2T_c} \right]^{2n-1} = 4\Lambda\mu \tanh \frac{\Lambda}{2T_c}.\end{aligned} \tag{A.24}$$

As a result, equation (A.21) becomes

$$2\alpha d(x) + 4T_c \left(\ln\cosh \frac{\Lambda+\mu}{2T_c} + \ln\cosh \frac{\Lambda-\mu}{2T_c} - 2\ln\cosh \frac{\mu}{2T_c} \right) - 4\Lambda\mu \tanh \frac{\Lambda}{2T_c} = 0. \tag{A.25}$$

Since $\Lambda \gg \mu$, one has

$$d(x) - \frac{2\mu\Lambda}{\alpha} \tanh \frac{\Lambda}{2T_c} + \frac{4\mu T_c}{\alpha} \left(\ln\cosh \frac{\Lambda}{2T_c} - \ln\cosh \frac{\mu}{2T_c} \right) = 0. \tag{A.26}$$

Plugging in the expression for the $\ln\cosh$-terms from equation (A.14) gives

$$d(x) - \frac{2\mu\Lambda}{\alpha} \tanh \frac{\Lambda}{2T_c} + \frac{2\mu}{Ng_S} = 0. \tag{A.27}$$

Taking again into account that $\Lambda \gg T_c$, so that $\tanh \Lambda/2T_c \approx 1$, substituting $g_c = \alpha/\Lambda$ and $\eta = 1 - g_c/Ng_S$, and solving for μ leads to equation (3.86).

Bibliography

[1] P Mangin and R Kahn. *Superconductivity: an introduction*. Springer, 2016.

[2] Heiko Thomas, Adela Marian, Alexander Chervyakov, Stefan Stückrad, Delia Salmieri, and Carlo Rubbia. Superconducting transmission lines–sustainable electric energy transfer with higher public acceptance? *Renewable and Sustainable Energy Reviews*, 55:59–72, 2016.

[3] Marc T Thompson and Richard D Thornton. Flux-canceling electrodynamic maglev suspension: part ii test results and scaling laws. *IEEE transactions on magnetics*, 35(3):1964–1975, 1999.

[4] H Kamerlingh Onnes. Further experiments with Liquid Helium. In *KNAW Proceedings*, pages 818–821. KNAW, 1912.

[5] J Bardeen, LN Cooper, and JR Schrieffer. Theory of superconductivity. *Physical review*, 108(5):1175, 1957.

[6] JG Bednorz and KA Müller. Possible high T_c superconductivity in the Ba-La-Cu-O system. *Zeitschrift für Physik B Condensed Matter*, 64(2):189–193, 1986.

[7] EC Marino. *Quantum field theory approach to condensed matter physics*. Cambridge University Press, 2017.

[8] P Ray. *Structural investigation of $La_{2-x}Sr_xCuO_{4+y}$ - Following staging as a function of temperature*. PhD thesis, Niels Bohr Institute, Copenhagen University., 11 2015.

[9] W Meissner and R Ochsenfeld. Ein neuer Effekt bei Eintritt der Supraleitfähigkeit. *Naturwissenschaften*, 21(44):787–788, 1933.

[10] JE Kunzler. Superconductivity in high magnetic fields at high current densities. *Reviews of Modern Physics*, 33(4):501, 1961.

[11] CA Reynolds, B Serin, and LB Nesbitt. The isotope effect in superconductivity. I. Mercury. *Physical Review*, 84(4):691, 1951.

[12] M Hoesch, T Fukuda, J Mizuki, T Takenouchi, H Kawarada, JP Sutter, S Tsutsui, AQR Baron, M Nagao, and Y Takano. Phonon softening in superconducting diamond. *Physical Review B*, 75(14):140508, 2007.

[13] M Krantz, HJ Rosen, RM Macfarlane, and VY Lee. Effect of oxygen stoichiometry on softening of Raman active lattice modes in $YBa_2Cu_3O_y$. *Physical Review B*, 38(7):4992, 1988.

[14] F London and H London. The electromagnetic equations of the supraconductor. *Proceedings of the Royal Society of London. Series A-Mathematical and Physical Sciences*, 149(866):71–88, 1935.

[15] HTC Stoof, KB Gubbels, and D Dickerscheid. *Ultracold quantum fields*. Springer, 2009.

[16] AL Fetter and JD Walecka. *Quantum theory of many-particle systems*. McGraw-Hill, 1971.

[17] DM Ginsberg. Encyclopædia Britannica: Superconductivity - Transition temperatures, 2018. Accessed: November 14, 2019.

[18] I Giaever and K Megerle. Study of superconductors by electron tunneling. *Physical Review*, 122(4):1101, 1961.

[19] D Ohlendorf and E Wicke. Heat capacities between 1.5 and 16 K and superconductivity of V/H and Nb/H alloys. *Journal of Physics and Chemistry of Solids*, 40(10):721–728, 1979.

[20] G Zhao, V Kirtikar, and DE Morris. Isotope effects and possible pairing mechanism in optimally doped cuprate superconductors. *Physical Review B*, 63(22):220506, 2001.

[21] JCS Davis and D Lee. Concepts relating magnetic interactions, intertwined electronic orders, and strongly correlated superconductivity. *Proceedings of the National Academy of Sciences*, 110(44):17623–17630, 2013.

[22] DJ Scalapino. A common thread: The pairing interaction for unconventional superconductors. *Reviews of Modern Physics*, 84(4):1383, 2012.

[23] J Yu, AJ Freeman, and J Xu. Electronically driven instabilities and superconductivity in the layered $La_{2-x}Ba_xCuO_4$ perovskites. *Physical review letters*, 58(10):1035, 1987.

[24] JL Wagner, BA Hunter, DG Hinks, and JD Jorgensen. Structure and superconductivity of $HgBa_2Ca_2Cu_3O_{8+\delta}$. *Physical Review B*, 51(21):15407, 1995.

[25] CNR Rao, L Ganapathi, R Vijayaraghavan, GR Rao, K Murthy, and R Ram. Superconductivity in the $Bi_2(Ca, Sr)_{n+1}Cu_nO_{2n+4}$ (n= 1, 2, or 3) series: Synthesis, characterization and mechanism. *Physica C: Superconductivity*, 156(5):827–833, 1988.

[26] G Dopf, A Muramatsu, and W Hanke. Consistent description of high-T_c superconductors with the three-band Hubbard model. *Physical review letters*, 68(3):353, 1992.

[27] JD Jorgensen. Defects and superconductivity in the copper oxides. *Physics Today*, 44:34–40, 1991.

[28] J Zaanen, GA Sawatzky, and JW Allen. Band gaps and electronic structure of transition-metal compounds. *Physical review letters*, 55(4):418, 1985.

[29] JB Torrance, Y Tokura, AI Nazzal, A Bezinge, TC Huang, and SSP Parkin. Anomalous Disappearance of High-T_c Superconductivity at High Hole Concentration in Metallic $La_{2-x}Sr_xCuO_4$. *Physical review letters*, 61(9):1127, 1988.

[30] KM Shen and JCS Davis. Cuprate high-T_c superconductors. *Materials today*, 11(9):14–21, 2008.

[31] M Buchanan. Mind the pseudogap, 2001.

[32] AA Kordyuk and SV Borisenko. ARPES on high-temperature superconductors: simplicity vs. complexity. *Low Temperature Physics*, 32(4):298–304, 2006.

[33] A Damascelli, Z Hussain, and Z Shen. Angle-resolved photoemission studies of the cuprate superconductors. *Reviews of modern physics*, 75(2):473, 2003.

[34] N Nücker, J Fink, B Renker, D Ewert, C Politis, PJW Weijs, and JC Fuggle. Experimental electronic structure studies of $La_{2-x}Sr_xCuO_4$. *Zeitschrift für Physik B Condensed Matter*, 67(1):9–14, 1987.

[35] E Dagotto. Correlated electrons in high-temperature superconductors. *Reviews of Modern Physics*, 66(3):763, 1994.

[36] VJ Emery. Theory of high-T_c superconductivity in oxides. *Physical Review Letters*, 58(26):2794, 1987.

[37] J Zaanen and O Gunnarsson. Charged magnetic domain lines and the magnetism of high-T_c oxides. *Physical Review B*, 40(10):7391, 1989.

[38] S Bulut, WA Atkinson, and AP Kampf. Spatially modulated electronic nematicity in the three-band model of cuprate superconductors. *Physical Review B*, 88(15):155132, 2013.

[39] N Nücker, J Fink, JC Fuggle, PJ Durham, and WM Temmerman. Evidence for holes on oxygen sites in the high-t c superconductors $La_{2-x}Sr_xCuO_4$ and $YBa_2Cu_3O_{7-y}$. *Physical Review B*, 37(10):5158, 1988.

[40] FC Zhang, C Gros, TM Rice, and H Shiba. A renormalised Hamiltonian approach to a resonant valence bond wavefunction. *Superconductor Science and Technology*, 1(1):36, 1988.

[41] W Hanke, ML Kiesel, M Aichhorn, S Brehm, and E Arrigoni. The 3-band Hubbard-model versus the 1-band model for the high-T_c cuprates: Pairing dynamics, superconductivity and the ground-state phase diagram. *The European Physical Journal Special Topics*, 188(1):15–32, 2010.

[42] J Spałek. tJ model then and now: a personal perspective from the pioneering times. *arXiv preprint arXiv:0706.4236*, 2007.

[43] H Eskes and R Eder. Hubbard model versus t-J model: The one-particle spectrum. *Physical Review B*, 54(20):R14226, 1996.

[44] A Fujimori. Lectures on strongly correlated systems using synchrotron radiation: Basics to frontiers, 2002. Accessed: January 26, 2020.

[45] VJ Emery and G Reiter. Reply to "Validity of the t-J model". *Physical Review B*, 41(10):7247, 1990.

[46] G Nikšić, I Kupčić, DK Sunko, and S Barišić. In-plane oxygens in high-temperature superconducting cuprates. *Journal of superconductivity and novel magnetism*, 26(8):2669–2673, 2013.

[47] M Reehuis, C Ulrich, K Prokeš, A Gozar, G Blumberg, S Komiya, Y Ando, P Pattison, and B Keimer. Crystal structure and high-field magnetism of La_2CuO_4. *Physical Review B*, 73(14):144513, 2006.

[48] LF Feiner, M Grilli, and C Di Castro. Apical oxygen ions and the electronic structure of the high-T_c cuprates. *Physical Review B*, 45(18):10647, 1992.

[49] L Adamska, MB Silva Neto, and C Morais Smith. Competing impurities in an antiferromagnetic background. *Bulletin of the American Physical Society*, 52, 2007.

[50] H Harashina, T Nishikawa, T Kiyokura, S Shamoto, M Sato, and K Kakurai. Cu-site doping effects, transport and magnetic properties of high-T_c oxides and their hole concentration dependence. *Physica C: Superconductivity*, 212(1-2):142–150, 1993.

[51] G Xiao, MZ Cieplak, JQ Xiao, and CL Chien. Magnetic pair-breaking effects: moment formation and critical doping level in superconducting $La_{1.85}Sr_{0.15}Cu_{1-x}A_xO_4$ systems (A= Fe, Co, Ni, Zn, Ga, Al). *Physical Review B*, 42(13):8752, 1990.

[52] MB Silva Neto, L Benfatto, V Juricic, and C Morais Smith. Magnetic susceptibility anisotropies in a two-dimensional quantum Heisenberg antiferromagnet with Dzyaloshinskii-Moriya interactions. *Physical Review B*, 73(4):045132, 2006.

[53] L Benfatto and MB Silva Neto. Field dependence of the magnetic spectrum in anisotropic and Dzyaloshinskii-Moriya antiferromagnets. i. theory. *Physical Review B*, 74(2):024415, 2006.

[54] Wikipedia. Percolation theory, 2019. Accessed: January 15, 2020.

[55] L Adamska, MB Silva Neto, and C Morais Smith. Competing impurities and reentrant magnetism in $La_{2-x}Sr_xCu_{1-z}Zn_zO_4$: Role of Dzyaloshinskii-Moriya and X Y anisotropies. *Physical Review B*, 75(13):134507, 2007.

[56] P Mainwood. I heard a percolation theory exhibits a second-order transition. How do you know that?, 2018. Accessed: February 2, 2020.

[57] E Fradkin. *Field theories of condensed matter physics*. Cambridge University Press, 2013.

[58] V Juricic. *Field-Theoretical Studies of a doped Mott Insulator*. PhD thesis, Utrecht University, 2006.

[59] Wikipedia. Spin stiffness, 2018. Accessed: April 1, 2020.

[60] EC Marino, RO Corrêa Jr, R Arouca, LHCM Nunes, and VS Alves. Superconducting and Pseudogap Transition Temperatures in High-T_c Cuprates and the T_c Dependence on Pressure. *Superconductor Science and Technology*, 33(3):035009, 2020.

[61] AP Kampf. Magnetic correlations in high temperature superconductivity. *Physics Reports*, 249(4-5):219–351, 1994.

[62] M Hücker, V Kataev, J Pommer, J Harraß, A Hosni, C Pflitsch, R Gross, and B Büchner. Mobility of holes and suppression of antiferromagnetic order in $La_{2-x}Sr_xCuO_4$. *Physical Review B*, 59(2):R725, 1999.

[63] M Hinczewski and AN Berker. Finite-temperature phase diagram of nonmagnetic impurities in high-temperature superconductors using a $d = 3$ t-J model with quenched disorder. *Physical Review B*, 78(6):064507, 2008.

[64] S Uchida. Zn-impurity effects on high-temperature superconductivity. *Physica C: Superconductivity*, 357:25–29, 2001.

[65] T Churei, H Hiraka, Y Endoh, M Matsuda, and K Yamada. Effect of magnetic impurities on superconductivity and spin correlation of $La_{2-x}Sr_xCuO_4$. *Physica C: Superconductivity*, 392:194–198, 2003.

[66] AM Finkel'stein, VE Kataev, EF Kukovitskii, and GB Teitel'Baum. Effects of Zn substitution for Cu atoms in lanthanum-strontium superconductors. *Physica C: Superconductivity*, 168(3-4):370–380, 1990.

[67] S Mukhopadhyay, G Sheet, AK Nigam, P Raychaudhuri, and H Takeya. Effect of Pt doping on the critical temperature and the upper critical field in $YNi_{2-x}Pt_xB_2C$ for doping range $0 < x < 0.2$. *Physical Review B*, 79(13):132505, 2009.

[68] P Hirschfeld, WO Putikka, and DJ Scalapino. d-wave model for microwave response of high-T_c superconductors. *Physical Review B*, 50(14):10250, 1994.

[69] JE Crow and RD Parks. The transition temperature of superconductors with paramagnetic impurities. *Physics Letters*, 21(4):378–379, 1966.

[70] M Park, MH Lee, and Y Kim. Impurity scattering in a d-wave superconductor. *Modern Physics Letters B*, 11(16n17):719–726, 1997.

[71] M Fujita, M Enoki, S Iikubo, K Kudo, N Kobayashi, and K Yamada. Gigantic Impact of Magnetic Impurity on Stripe Order in $La_{2-x}Sr_xCuO_4(x \sim 1/8)$. *arXiv preprint arXiv:0903.5391*, 2009.

[72] RS Islam and SH Naqib. Zn induced in-gap electronic states in La214 probed by uniform magnetic susceptibility: relevance to the suppression of superconducting T_c. *Superconductor Science and Technology*, 31(2):025004, 2017.

[73] B Nachumi, A Keren, K Kojima, M Larkin, GM Luke, J Merrin, O Tchernyshöv, YJ Uemura, N Ichikawa, M Goto, et al. Muon spin relaxation studies of Zn-substitution effects in high-T_c cuprate superconductors. *Physical review letters*, 77(27):5421, 1996.

[74] AM Valente, P Darriulat, CA Van 't Hof, MA Peck, S Calatroni, and C Benvenuti. Study of the Residual Resistance of Superconducting Niobium Films at 1.5 GHz. Technical report, CERN, 1999.

[75] Y Fukuzumi, K Mizuhashi, K Takenaka, and S Uchida. Universal superconductor-insulator transition and T_c depression in Zn-substituted high-T_c cuprates in the underdoped regime. *Physical review letters*, 76(4):684, 1996.

[76] M Julien, T Fehér, M Horvatić, C Berthier, ON Bakharev, P Ségransan, G Collin, and J Marucco. 63-Cu NMR Evidence for Enhanced Antiferromagnetic Correlations around Zn Impurities in $YBa_2Cu_3O_{6.7}$. *Physical review letters*, 84(15):3422, 2000.

[77] P Mendels, J Bobroff, G Collin, H Alloul, M Gabay, JF Marucco, N Blanchard, and B Grenier. Normal-state magnetic properties of Ni and Zn substituted in $YBa_2Cu_3O_{6+x}$: Hole-doping dependence. *EPL (Europhysics Letters)*, 46(5):678, 1999.

[78] RS Islam, JR Cooper, JW Loram, and SH Naqib. On the pseudogap and doping-dependent magnetic properties of $La_{2-x}Sr_xCu_{1-y}Zn_yO_4$. *Physica C: Superconductivity*, 460:753–755, 2007.

[79] J Tallon, C Bernhard, GVM Williams, and JW Loram. Zn-induced T_c reduction in High-T_c Superconductors: Scattering in the Presence of a Pseudogap. *Physical review letters*, 79(26):5294, 1997.

[80] C Morais Smith, AH Castro Neto, and AV Balatsky. T_c Suppression in Co-Doped Striped Cuprates. *Physical review letters*, 87(17):177010, 2001.

[81] D Poilblanc, DJ Scalapino, and W Hanke. Resonant impurity scattering in a strongly correlated electron model. *Physical review letters*, 72(6):884, 1994.

[82] J Zhu and CS Ting. Local quasiparticle states near a Zn impurity with induced magnetic moment in a high-T_c superconductor. *Physical Review B*, 64(6):060501, 2001.

[83] R Yoshizaki, N Ishikawa, H Sawada, E Kita, and A Tasaki. Magnetic susceptibility of normal state and superconductivity of $La_{2-x}Sr_xCuO_4$. *Physica C: Superconductivity*, 166(5-6):417–422, 1990.

[84] T Kluge, Y Koike, A Fujiwara, M Kato, T Noji, and Y Saito. Clear distinction between the underdoped and overdoped regime in the T_c suppression of Cu-site-substituted high-T_c cuprates. *Physical Review B*, 52(2):R727, 1995.